H2S Regulates Hypobaric Hypoxia-Induced Early Glio-Vascular Dysfunction and Neuro-Pathophysiological Effects

10 authors, including:

Gaurav Kumar
Chhatrapati Shahu Ji Maharaj University
20 PUBLICATIONS   114 CITATIONS

SEE PROFILE

Aastha Chhabra
Defence Institute of Physiology and Allied Sciences, DRDO, Delhi
23 PUBLICATIONS   330 CITATIONS

SEE PROFILE

Shalini Mishra
Defence Research and Development Organisation
24 PUBLICATIONS   127 CITATIONS

SEE PROFILE

Haroon Kalam
Broad Institute of MIT and Harvard
36 PUBLICATIONS   383 CITATIONS

SEE PROFILE

Research Paper

H$_2$S Regulates Hypobaric Hypoxia-Induced Early Glio-Vascular Dysfunction and Neuro-Pathophysiological Effects

Gaurav Kumar [a], Aastha Chhabra [b], Shalini Mishra [b], Haroon Kalam [c], Dhiraj Kumar [c], Ramniwas Meena [b], Yasmin Ahmad [b], Kalpana Bhargava [b], Dipti N. Prasad [a], Manish Sharma [b],*

[a] Neurobiology Division, Defence Institute of Physiology and Allied Sciences (DIPAS), DRDO, Delhi 110054, India
[b] Peptide and Proteomics Division, Defence Institute of Physiology and Allied Sciences (DIPAS), DRDO, Delhi 110054, India
[c] Immunology Group, International Center for Genetic Engineering and Biotechnology (ICGEB), Aruna Asaf Ali Marg, New Delhi-110067, India

ABSTRACT

Hypobaric Hypoxia (HH) is an established risk factor for various neuro-physiological perturbations including cognitive impairment. The origin and mechanistic basis of such responses however remain elusive. We here combined systems level analysis with classical neuro-physiological approaches, in a rat model system, to understand pathological responses of brain to HH. Unbiased 'statistical co-expression networks' generated utilizing temporal, differential transcriptome signatures of hippocampus—centrally involved in regulating cognition—implicated perturbation of Glio-Vascular homeostasis during early responses to HH, with concurrent modulation of vasomodulatory, hemostatic and proteolytic processes. Further, multiple lines of experimental evidence from ultra-structural, immuno-histological, substrate-zymography and barrier function studies unambiguously supported this proposition. Interestingly, we show a significant lowering of H$_2$S levels in the brain, under chronic HH conditions. This phenomenon functionally impacted hypoxia-induced modulation of cerebral blood flow (hypoxic autoregulation) besides perturbing the strength of functional hyperemia responses. The augmentation of H$_2$S levels, during HH conditions, remarkably preserved Glio-Vascular homeostasis and key neuro-physiological functions (cerebral blood flow, functional hyperemia and spatial memory) besides curtailing HH-induced neuronal apoptosis in hippocampus. Our data thus revealed causal role of H$_2$S during HH-induced early Glio-Vascular dysfunction and consequent cognitive impairment.

© 2016 The Authors. Published by Elsevier B.V. This is an open access article under the CC BY-NC-ND license (http://creativecommons.org/licenses/by-nc-nd/4.0/).

1. Introduction

Amongst various organ systems, central nervous system (CNS) is highly vulnerable to hypoxic insult, owing to its high-energy requirements (Ladecola, 2013) and thus, ensuing risk of compromised function (Wilson et al., 2009). Several pathological states including asphyxia, stroke, head injury besides environmental conditions, such as those encountered at high altitude, culminate in reduced oxygen availability to brain cells (Wilson et al., 2009). Hypobaric Hypoxia (HH) resulting from reduction in the effective concentration of inspired Oxygen, due to decreased atmospheric pressure (with ascent to high altitude), culminates into various neuro-pathological conditions including distinctive cognitive impairment. Given the systemic nature of stress induced by HH, while it is conceivable that the neuro-pathological effects under these conditions are cumulative manifestations of tissue-specific (brain) responses and paracrine factors of distant tissue origin (secreted in plasma); the precise molecular, patho-etiological basis of such effects remain elusive. It is noteworthy that besides an immediate relevance for well being at altitude; research in this area promises a unique opportunity to decipher facts, which can also be applied to critical care medicine (Grocott et al., 2007). For such reasons, thus, the mechanistic understanding of this phenomenon has remained the Holy Grail for numerous basic and clinical researchers across the globe since several decades.

The early phases of HH-induced physiological response result in the activation of various adaptive measures at systemic (Imray et al., 2010; Teppema and Dahan, 2010; West et al., 2007), cellular and metabolic levels (Harik et al., 1995). The chronic exposure, however, culminates in conspicuous pathological outcomes related to brain, ranging from moderate to severe forms, in a time- and exposure-dependent manner (Bartsch and Swenson, 2013; Dehnert et al., 2007; Hackett and Roach, 2004; Imray et al., 2010; Sylvester et al., 2012; Willmann et al., 2014; Yan, 2014). The moderate neurological effects of sustained HH include Acute Mountain Sickness (AMS), insomnia, dizziness and alteration of mood (Hackett and Roach, 2001; Wilson et al., 2009) while the severe

forms, possibly due to chronic maladaptation to HH, include clinical conditions such as long term impairment of psychomotor (Bouquet et al., 1999; Virues-Ortega et al., 2004) and cognitive functions (Kramer et al., 1993; Yan, 2014) besides dire, life threatening consequences arising from high altitude cerebral edema (HACE) (Hackett and Roach, 2004; Hackett et al., 1998; Schommer et al., 2013; Willmann et al., 2014; Wilson et al., 2009).

The neuro-pathological alterations in response to HH are variously attributed to oxidative stress (Maiti et al., 2006), modulation of cholinergic markers (Muthuraju et al., 2011), excitotoxicity (Hota et al., 2008; Mark et al., 2001) and dendritic atrophy in hippocampal pyramidal neurons (Titus et al., 2007). Notably, however, the molecular mechanistic basis of HH-induced changes in neurophysiology and ensuing cognitive impairments is grossly lacking. We here utilized a rat model system of HH and performed temporal, genome-wide expression profiling followed by unbiased statistical networking in conjunction with biological pathway mining strategies to infer chronology of physiological/molecular perturbations during HH-induced neuro-pathological effects. Our data yielded unambiguous evidence for the perturbation of Glio-Vascular units during early response to HH, which progressed to modulate Neuro- vascular unit function and cognitive impairment. We implicate complex molecular circuitry involving modulation of multiple regulators of Calcium sensitivity and vascular homeostasis prior to disruption of such basic 'units of function' in the brain. Interestingly, we show that marked reduction in H_2S levels in the brain causally governed neuro-vascular dysfunction and ensuing pathophysiological effects of HH.

2. Materials and Methods

2.1. Animal Experiments and Ethics Statement

Male Sprague Dawley rats weighing 225–250 g were used for the study. The animals were maintained in animal house facility of the institute and were exposed to 12 h each of light–dark cycle. The animals were fed with pellet diet and water *ad libitum*. The study design was approved by the standing 'Institute Animal Ethics Committee' of Defence Institute of Physiology and Allied Sciences (DIPAS), Delhi and the experiments were conducted in strict compliance with the guidelines of 'Committee for the Purpose of Control and Supervision of Experiments on Animals (CPCSEA)', Government of India.

2.2. High Altitude Simulation (Hypobaric Hypoxia Exposure)

The animals were exposed to simulated-high altitude (Hypobaric Hypoxia, HH) in a specially designed animal decompression chamber to maintain a constant pressure of 282 Torr (equivalent to an altitude of 7620 m, 8% O2). The rate of ascent and descent to hypobaric condition was maintained at 300 m/min. Fresh air was constantly flushed in at a rate of 8 L/min to prevent accumulation of CO2 within the chamber. The temperature and humidity in the chamber were maintained at 28 ± 2 °C and 55–60%, respectively. The animals were randomly divided into desired groups (as explained in the Results section) with 5 animals in each group. The control groups were kept at normal atmospheric pressure (Normoxic control) under similar conditions.

2.3. Administration of H_2S Donor

The animals, in designated groups, received daily intra-peritoneal (i.p.) injection of Sodium hydrogen sulfide (NaHS·xH2O, Cayman Chemicals) at 4 mg per kg of body weight per day for 10 days prior to HH exposure. NaHS (2 mg/mL) was prepared fresh in 0.15 M phosphate-buffered saline (PBS) pH 7.4 before each injection. Parallel sham injections with equal volume of 0.15 M PBS were made in the control groups.

2.4. Morris Water Maze (MWM) Test

MWM test to assess spatial reference memory was performed as per published protocol (Vorhees and Williams, 2006) and described in detail in the Supplemental Text.

2.5. T-Maze Test

For alternative test of cognition, 'Rewarded Alternation Test' was performed employing T-Maze, as per published protocol (Deacon and Rawlins, 2006) and described in Supplemental Text.

2.6. Intracellular Cleaved-Caspase 3 Staining, TUNEL, Flow Cytometry, In Situ TUNEL, NOx and cGMP Estimation

These assays were performed utilizing commercially available kits and standard protocols described in Supplemental Text.

2.7. Microarray Analysis

One-color microarray based gene expression analysis was performed utilizing Agilent microarray platform and all raw data sets were submitted to GEO (Accession number: GSE66287). Experimental design, sampling, hybridization and data analysis were performed in strict compliance with Minimum Information About a Microarray Experiment (MIAME) guidelines. Data pre-processing and differential expression analysis was conducted by R software using Bioconductor packages as reported previously (Sharma et al., 2014) and described in Supplemental Text.

2.8. Bioinformatic Analysis

Gene Ontology (GO), Pathway Mining, and Functional Annotation Clustering was done utilizing DAVID Bioinformatics resource (NIAID, NIH). Gene MANIA (Warde-Farley et al., 2010) (as Cytoscape plug-in) was used to extract functional networks representing non-redundant, statistically significant biological processes, depicted as degree sorted circular view. This tool caters a unique advantage with the output networks from a query gene list principally based on well-established, experimentally inferred expression data sets from published studies. The over- represented groups of GO and functional terms were established utilizing software 'BiNGO' (as a Cytoscape plug-in).

2.9. Weighted Gene Co-Expression Network Analysis (WGCNA)

R package was used for executing WGCNA as described in (Langfelder and Horvath, 2008) and briefly described in Supplemental Text.

2.10. Transmission Electron Microscopy, Gelatin Zymography, Western Blotting, Histological Analysis, Immunohistochemistry, Immunofluorescence

These assays were performed as per standard protocol and described in Supplemental Text.

2.11. BBB Permeability (Sodium Fluorescein Extravasation Assay)

The assay was performed as per protocol described previously (Phares et al., 2006).

2.12. Estimation of Sulfide Levels by Zinc Precipitation Assay

Total free sulfide estimation in tissue samples was done as per published protocol (Ang et al., 2012) and described briefly in Supplemental Text.

2.13. Cerebral Blood Flow Measurements and Functional Hyperemia Studies

Cerebral blood flow (CBF) was measured utilizing Laser Doppler Flowmetry (LDF), as per published protocol (Sutherland et al., 2014) and briefly, described in Supplemental Text. It measures blood perfusion across the region of interest by estimating total blood cell flux (RBCs) traversing this region in a specific duration of time. The total blood cell flux is expressed as Blood Perfusion Units (BPU)—arbitrary units proportional to the product of mean velocity and number of blood cells traversing this region. Whisker Stimulation method was employed for assessing functional hyperemia responses, as per protocol described in Supplemental Text.

2.14. Statistics

The datasets from independent experiments (N ≥ 3) were represented either as Mean ± SEM, Box-Whisker Plots (with Median Values) or Dot Plots (with Mean ± SEM). The statistical significance of individual parameters within multiple groups of specific experiment was evaluated by one-way analysis of variance (*P < 0.05, **P < 0.01, ***P < 0.001). At specific instances (as noted in figure legends), Bonferroni multiple comparison test was conducted as a post-hoc analysis.

3. Results

3.1. Hypobaric Hypoxia (HH) Induces Spatial Memory Impairment Concomitant with the Loss of Hippocampal Neurons

We began by establishing the time window, during which HH-induced significant deficit in spatial memory manifests in the 'trained animals' (utilizing Morris Water Maze Test). The experimental strategy for this test is schematically represented in Fig. 1A. As shown in Fig. 1B & C, time taken by the animals (Latency) to reach the platform, and path length covered to reach it, constantly decreased with each day during the 5 days training regimen prior to exposure to hypobaric hypoxia. Notably; in stark contrast to the animals kept in Normoxic environment subsequent to training, the exposure of animals to 7 days of Hypobaric
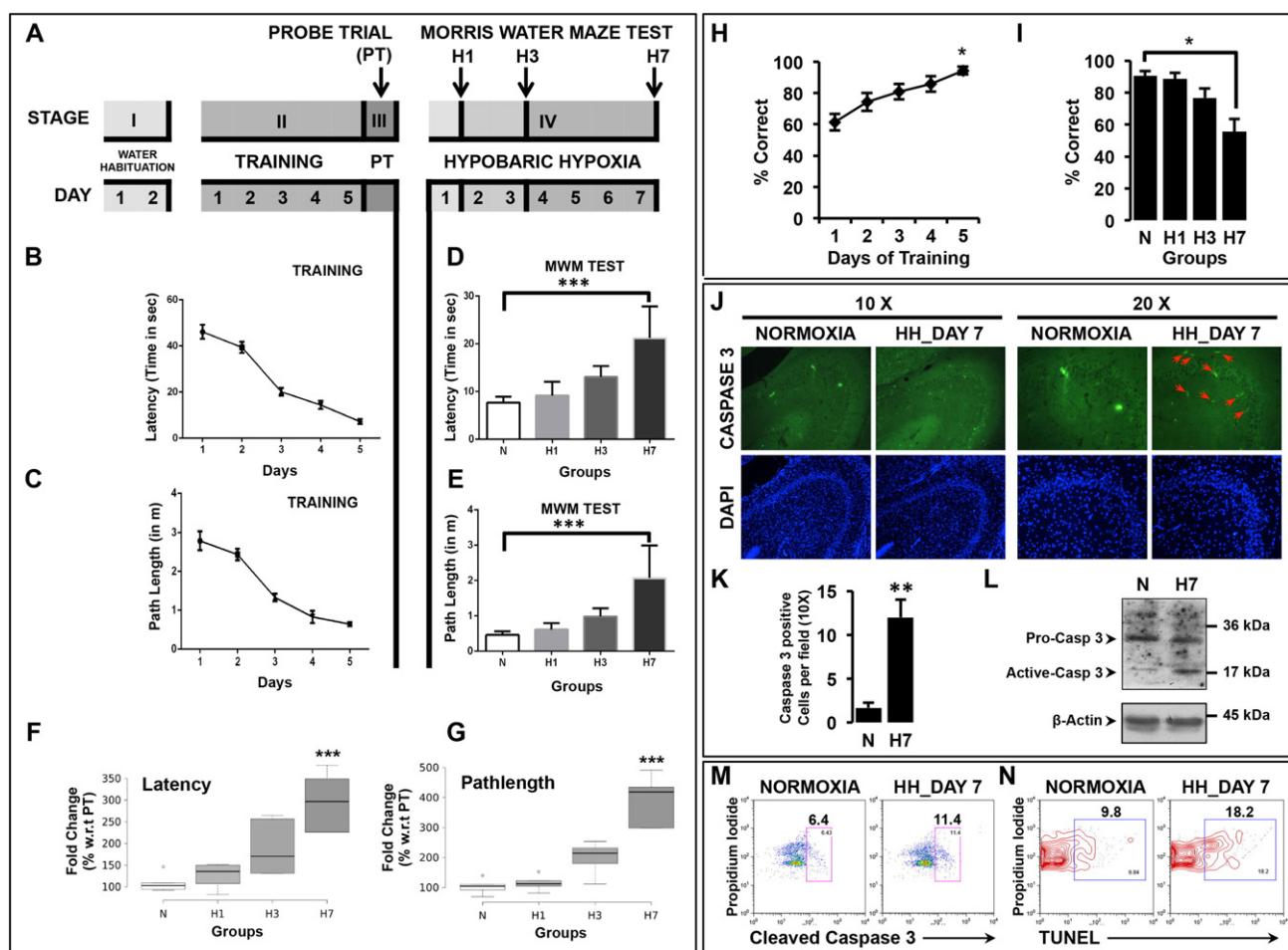
Fig. 1. Hypobaric Hypoxia induces spatial memory impairment concomitant with the loss of Hippocampal neurons during HH A) Schematic representation of the experimental strategy utilized for Morris Water Maze test. Training of the animals consisted of two days of water habituation, five days of training followed by probe trial prior to Hypobaric Hypoxia exposure for indicated duration of time. B) Line graph depicting Latency (Time taken (in seconds) to reach the platform), and C) Path Length (Distance (in m) travelled by the rat to first hit the platform area). Mean ± S.D. is shown. D) Bar graph representing Latency and E) Path Length parameters in MWM tests (Mean ± S.D.). F) Box-and-whisker plot showing percentage change in Latency and G) Path length parameters in MWM test with respect to the performance of same animal during probe trial. H) Line graph depicting time-dependent learning of rewarded alternation task in elevated T-Maze. I) Bar graph representing performance of animals in T-Maze test, after indicated duration of exposure to HH. J) Immunofluorescence micrographs (10× & 20×) showing cleaved-Caspase 3-positive cells (Alexa fluor 488, Green) from hippocampal region of brain from animals kept in Normoxia or 7 days of HH. The sections were also counterstained with DAPI (Blue) to indicate location of cells. DAPI staining pattern for respective regions is shown below Caspase-3 panels (labeled in figure). K) Bar graph representing average number of active (Cleaved) Caspase 3-positive cells per microscopic field (10×). L) Representative image of Western blotting (Caspase 3) in extracts prepared from hippocampal region of animals kept in Normoxia or 7 days of HH. Flow Cytometry analysis: M) Intracellular cleaved-Caspase 3 staining N) TUNEL staining, in cells isolated from hippocampal tissues of animals kept in Normoxia or 7 days of Hypobaric Hypoxia. Statistical significance of specific parameters shown in the figure was evaluated by one-way analysis of variance (*P < 0.05, ***P < 0.001). Bonferroni multiple comparison test was conducted as a post-hoc analysis. (Abbreviations: N: Normoxic control, H1, H3 & H7: 1, 3 & 7 days, post Hypobaric Hypoxia (HH) exposure) (For interpretation of the references to colour in this figure legend, the reader is referred to the web version of this article.).

Hypoxia (H7) led to a significant deficit in spatial memory as indicated by increase in the average value of latency and path length for this group (Fig. 1D & E). To account for the intra-group variations in the responses of individual animals, we also calculated the change in latency and path length for individual animals, post hypoxia, in comparison to reference values for the same animal during probe trial, PT (refer methods for details). As shown in the box-whisker plots in Fig. 1F & G, we observed a significant increase (p < 0.001) in the median value for latency and path length in H7 group.

As an additional test of cognition and hippocampal function; we also monitored the animals for rewarded alternation tasks, utilizing elevated T-maze (Deacon and Rawlins, 2006), following Hypobaric Hypoxia exposure. Fig. 1H shows the day-wise pattern of learning (mean % correct). The animals, with each day of training, progressively learnt to perform the task, reaching a score ≥85% on the fifth day (Fig. 1H). Subsequently, the designated groups of animals were exposed to Hypobaric Hypoxia for 1, 3 and 7 days, respectively and tested for their ability to recapitulate rewarded alternation task. As shown in Fig. 1I, 7 days of Hypobaric Hypoxia significantly impacted the performance of these (trained) animals in executing this task and thus, corroborating the effect of extended Hypobaric Hypoxia exposure on cognitive function.

To study the effect of chronic hypoxia on viability of the brain cells, we performed Caspase 3 staining and TUNEL assay. Fig. 1J shows representative immunofluorescence images for cleaved-Caspase 3 (active form) staining in the hippocampal region (critical for memory and cognition) of animals exposed to Normoxia or 7 days of HH. We observed a significant increase in the number of cleaved-Caspase 3-positive foci (Fig. 1J & K) in this region. Interestingly, as evident from the images shown in Fig. 1J, we observed relatively higher number of Caspase 3-positive cells in hippocampal CA3 region—known to predominantly contain pyramidal neuron bodies. To further support HH-induced Caspase 3 activation in this region, we also performed western blotting utilizing hippocampal tissue extracts (Fig. 1L) besides intracellular cleaved-Caspase 3 staining (Flow Cytometry) in the cells isolated from hippocampal region (Fig. 1M). Both these experiments independently supported activation of Caspase 3 in the hippocampal cells, after 7 days of exposure to HH. Further, *in situ* TUNEL assay in cells (Flow Cytometry) isolated from the hippocampal tissue (Fig. 1N) yielded direct evidence for increased number of apoptotic cells in this region. In view of apoptotic events in the region composed of pyramidal neurons, it appears likely that HH affects the viability of pyramidal neurons in hippocampal region.

3.2. Weighted Gene Coexpression Network Analysis Suggests HH-Induced Early Vascular Dysfunction

To capture temporal dynamics of hypoxia responses in hippocampus, we next generated global gene expression signatures after 1, 3 and 7 days of hypoxia exposure (Supplemental Tables 1, 2 & 3) and subjected this data to multiple analysis strategies (depicted diagrammatically in Fig. 2A). Interestingly, the principal component analysis (PCA) (Fig. 2B), hierarchical clustering (Fig. 2C) and sample dendrogram in

correlation with traits value represented as trait heat map, (Fig. 2D) clearly segregated day 1 data set from days 3 and 7. These observations strongly suggested plausible unique nature of responses at day 1.

We, therefore, generated a matrix with expression values of genes differentially modulated across various time points (days 1, 3 & 7) and subjected this array to an elegant statistical networking tool, Weighted Gene Coexpression Network Analysis (WGCNA) (Langfelder and Horvath, 2008). This tool generated inter-genic interactions based on the correlation between respective time-dependent expression patterns of various genes and did not consider *a priori* biological information for network construction. As shown in notable previous publications (Langfelder and Horvath, 2008; Oldham et al., 2006, 2008), such analysis potentially segregates cell-type specific and/or biological process-specific modules having unique expression patterns across various time points. With our data set, the initial weighted gene co-expression network construction returned 9 modules, represented with unique color codes in Fig. 2E. Fig. 2F illustrates the hierarchical clustering of different modules based on their specific Eigengene value. We, subsequently, fused modules with an Eigengene value <0.1 to obtain 6 modules significantly different from each other and represented these with a unique color code in Fig. 2G. As noted above, the genes within specific modules were expected to have unique co-expression patterns and hence, likely to compose a distinct biological entity (process/cell type). As an initial test for the modules constructed in our analysis, we sought to establish module trait relationship based on correlation between module Eigengene and specific spatial memory traits (latency and path length) recorded in our experiments. This analysis showed significant correlation values (close to +1 & −1) between pink and brown module with the two traits in question (Fig. 2H). We then grossly ascribed a biological identity to individual modules by superimposing Gene Ontology (GO) information on individual modules. As evident from the perfuse forced directed clustering of GO terms from various modules (shown in Fig. 2I); the two modules (pink and brown), having highest correlation values with spatial memory traits (described above), contained sub-clusters of biological processes including cognition, sensory perception, neuron development and morphogenesis. This observation underscored the gross functional relevance of modules constructed by WGCNA from within our temporal gene expression data set.

Interestingly, the green module was principally composed of GO terms related to cellular signaling regulating Vascular tone (Calcium Ion homeostasis, cyclic nucleotides, GPCRs and Catecholamine metabolism and smooth muscle contraction) while the blue module primarily contained other broad key terms related to vasculature (Angiogenesis, Smooth muscle proliferation and Junctional maintenance). Red and black modules did not return GO terms, which clustered to compose unique biological processes and hence, excluded from the current description. Taken together, WGCNA analysis segregated key biological processes, and specific clusters of genes regulating them, from amongst complex temporal expression patterns in hypoxic brain.

The module 'Eigengene' value represents a gross measure of module perturbation at a specific stage (time point in our case). To understand the temporal kinetics of various biological processes associated with

Fig. 2. Weighted Gene Coexpression Network Analysis (WGCNA) of time series global expression data. A) Scheme of data mining employed for analyzing microarray data. The lists of differentially expressed genes were subjected to various softwares including DAVID (Online resource), BiNGO and GeneMANIA (as Cytoscape plugins) besides Weighted Gene Coexpression Network Analysis (WGCNA). The biological networks were then represented as 'Degree sorted circular view' and GO networks as 'Perfused forced directed clusters'. B) Principal Component Analysis (PCA) of gene expression data sets from the hippocampus of animals exposed to HH (Days 1, 3 and 7) and Normoxia (Control) represented as two dimensional plot of PC1 (Component 1) and PC2 (Component 2). C) Hierarchical clustering of gene expression data. Color intensities correspond to log2 expression values of individual genes. D) Clustering dendrogram of samples based on their Euclidean distance. The trait Heat Map is depicted the Path Length and Latency parameter of MWM test. E) Modules (represented with unique color) corresponding to branches of cluster tree generated from clustering dendrogram of genes with dissimilarity based on topological overlap. F) Dendrogram obtained by clustering of module Eigengenes with dissimilarity based on topological overlap. Red line indicates cut-off value (0.1) G) Cluster dendrogram showing merged module with Eigengene value <0.1 represented by unique color. The original module color (as shown in panel E, utilized for dynamic tree cut) is also included for reference. H) Module-trait association plot representing relationship of modules with Latency (Time taken to reach the platform, in seconds) and Path Length (Distance (in m) travelled by the rat to reach the platform). Rows correspond to module Eigengene while columns to Latency and Path Length. Respective correlation and p-values are indicated in each cell. I) Clustered, over-represented groups of GO and functional terms identified from various modules using hyper geometric test in BiNGO (Cytoscape plug-in). The figure indicates gross annotation for GO term clusters identified by boxes. J) The top panel shows the bar graph obtained by plotting module Eigengene value (y-axis) plotted against time (HH Days 1, 3 & 7). The bottom panel represents heat map of expression values of genes composing respective modules (For interpretation of the references to colour in this figure legend, the reader is referred to the web version of this article.).
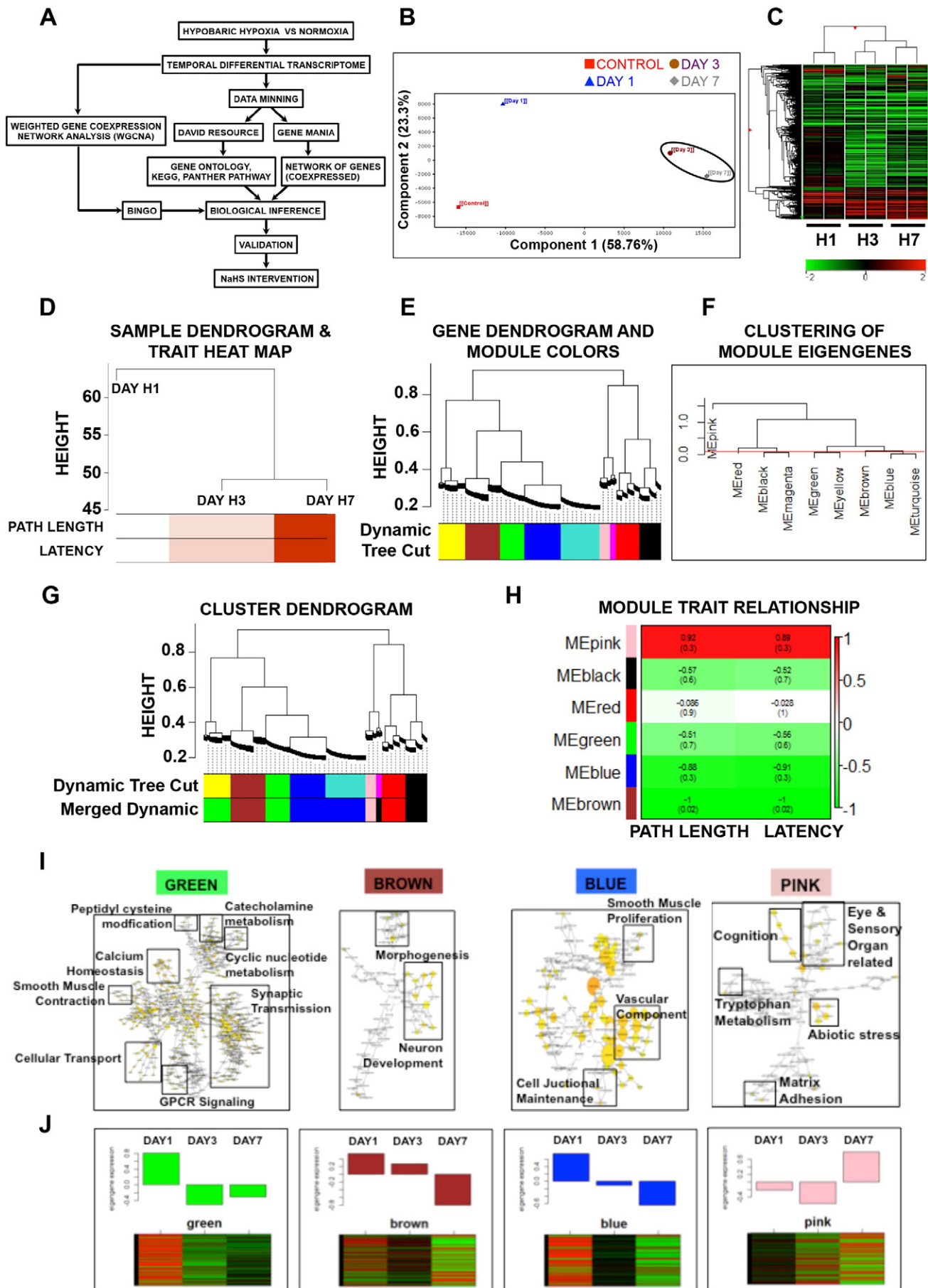
distinct modules, we plotted the Eigengene values of various modules along with heat map of expression values of specific genes composing these modules at all three time points (Fig. 2J). This data showed several interesting observations. The green and blue modules, which were principally composed of GO terms related to vascular components and related signaling processes, showed maximum perturbation at day 1 (Note the Eigengene values and expression patterns of module genes shown as heat maps). In stark contrast, pink and brown modules, which were composed of terms related to neurons, showed maximum perturbation and expression of respective genes by day 7. Taken together, these observations revealed several facts and raised some interesting possibilities: 1) Vascular dysfunction appeared to manifest early (at day 1) in response to HH 2) It temporally preceded perturbation of neuronal processes evident at day 7, post HH 3) Vascular dysfunction, an apparently early event, could play a causal role in initiating the cascade culminating in neuro-physiological perturbations (cognitive deficit) in response to HH.

3.3. Evidence for Involvement of Multiple Vasomodulatory Mediators during HH-Induced Early Vascular Injury

To further validate temporal segregation of responses as inferred by WGCNA analysis, we extracted gene networks enriched at individual time-points utilizing a vividly reported biological network construction tool, 'Gene MANIA' (Warde-Farley et al., 2010). Fig. 3 shows degree sorted circular view of key networks (biological co-expression and co-localization) representing non-redundant, statistically significant biological processes at day 1 (post HH). In agreement with the GO term clustering of Blue and Green Modules (having maximum perturbation at day 1, Fig. 2J), this analysis also showed enrichment of biological networks regulating blood pressure, vessel size and development, Calcium homeostasis, corticosteroid responses, Wound healing (including hemostasis/angiogenesis), Extracellular Matrix dynamics, Corticosteroid responses, leukocyte migration/activation, Cell adhesion and morphogenesis at day 1. Notably, biological networks related to core neurological processes such as regulation of behavior, Neuron projection, Nerve Transmission, Dendritic spine showed up only in day 3 and 7 data sets (Supplemental Figs. 1 & 2; Supplemental Tables 4 & 5), corroborating inferences drawn from WGCNA analysis. Taken together, these data sets reinforced the possibility that HH induces vascular dysfunction and injury with plausible sequelae of corticosteroid response, wound healing, coagulation/hemostatic processes involving platelets/leukocyte activation and ECM dynamics during early responses (day 1).

In view of unique nature of responses at day 1 (Fig. 2) and likely, causal role in cascade of events culminating in neuro-pathological effects of hypoxia (Figs. 2 & 3); we performed several additional analyses on this data set. Table 1 shows the canonical 'KEGG' and 'Panther' pathways extracted from the list of differentially expressed genes at day 1. As clearly observed from this list, the top statistically significant pathways included Coagulation and hemostasis, Calcium homeostasis, Smooth muscle contraction, Steroid hormone synthesis and GPCR signaling pathways transducing signals from vascular tone modulators including Endothelin, Angiotensin, Catecholamines (Epinephrine/Norepinephrine), Dopamine and 5-HT. Besides this, the data was suggestive of involvement of different classes of heterotrimeric G- proteins. Most of these pathways modulate Actomyosin organization and 'Calcium Sensitivity' in various cell types, including vascular smooth muscle, endothelial and neurons. In consequence, these pathways regulate diverse biological processes such as vascular tone, axon guidance and cell migration amongst several others. Notably, the data also suggested modulation of Gap junctions, Focal adhesion, Integrin and TGF-β receptor signaling—known to be involved in ECM dynamics, cell–cell communication, structural and functional tissue integrity. It thus appeared reasonable that the resultant of HH-induced multiple vasomodulatory cues converging on cellular 'Calcium Sensitivity' via GPCR pathways causally governed the onset of early vascular injury. This injury, in likely consequence, modulated ECM-

dynamics via multiple receptors and pathways involved in structural maintenance of tissues.

3.4. Ultra-Structural and Histological Evidence for the Early 'Glio-Vascular' Unit Perturbation

The likely involvement of vascular injury and tissue remodeling prompted us to investigate ultra-structural changes in rat brain after days 1, 3 & 7, post HH exposure. Fig. 4A shows the Electron micrographs of rat brain sections, post Hypobaric Hypoxia exposure. A careful analysis of these images revealed two striking observations: First, there was evidence for Astrocyte end feet swelling and second, the width of basement membrane (BM), as measured in high resolution EM images, was significantly lower than that observed in Normoxic animal (Fig. 4B). These observations suggested perturbation of 'Glio-Vascular' organization under hypoxic condition. As described in a logical order below, we additionally studied various phenomena—which could either corroborate or manifest as a consequence of such Glio-Vascular dysfunction.

The Astrocyte end feet swelling could likely be suggestive of its activation—marked by increase of GFAP expression in these cells. We therefore performed immunofluorescence and western blotting experiments utilizing specific antibody against rat GFAP. A representative IF staining is shown in Fig. 4C and mean expression from 3 independent experiments (estimated by intensity thresholding method utilizing Image J) in Fig. 4D. The western blotting result for GFAP expression is shown in Fig. 4E. We reproducibly observed significant increase in the expression of GFAP in response to hypoxia, suggesting activation of Astrocytes under these conditions.

Several previous studies (related to Stroke, Ischemic Brain Injury amongst others) had shown that the increased activity of Serine Proteases (Tissue Plasminogen Activator (tPA), Urokinase) and Matrix Metalloproteinases (MMPs) is causally linked to degradation of ECM proteins—critically required to maintain basement membrane (BM) (Hermann and ElAli, 2012). We were thus prompted to study MMP activities under various conditions, utilizing Gelatin- and Casein-substrate zymography. The representative Gelatin zymography results, utilizing brain extracts, are depicted in Fig. 4F. We observed a significant increase in the activity of MMP 9 in brain extracts from animals exposed to 1 day of hypobaric hypoxia. This activity, however, decreased at the subsequent time points analyzed. The activity of MMP 2 did not show much change in response to HH. The specificity of matrix metalloproteinase activity was established by employing two inhibitors of MMPs, o-Phenanthroline and EDTA (Fig. 4F). We could not detect any MMP 8 activity, either in normoxic or hypoxic samples, at any time point in our casein zymography experiments. Taken together, these experiments showed increase in MMP 9 activity during early hypoxia responses. The increase in this activity did not appear to be regulated at the level of transcription, as inferred from the lack of MMP 9 transcript within differentially expressed genes at day 1, 3 or 7. Notably, however, the expression of tPA (PLAT), known to promote MMP 9 activity, was increased at all time points in our data set (Fig. 4G).

The erosion of basement membrane and activation of Astrocytes could be causally linked to possible endothelial dysfunction/activation. To investigate this possibility, we performed vWF staining—a marker of endothelial activation. As evident from representative IHC images depicted in Fig. 4H and average expression in each group in Fig. 4I, we observed a time-dependent increase in vWF expression in hypoxic rat brain. Notably, our transcriptome data also showed increase in transcript for vWF at all time points studied. Furthermore, increased expression of soluble ICAM-1 (sICAM-1) is also suggested to be a surrogate 'plasma marker' of endothelial activation. To further support our observation of HH-induced endothelial activation, we performed western blotting with plasma samples from animals exposed to HH. As shown in Fig. 4J, we clearly observed increase in sICAM-1 in a time dependent manner on exposure to HH. Taken together, these observations clearly suggested an early endothelial dysfunction in response to HH.
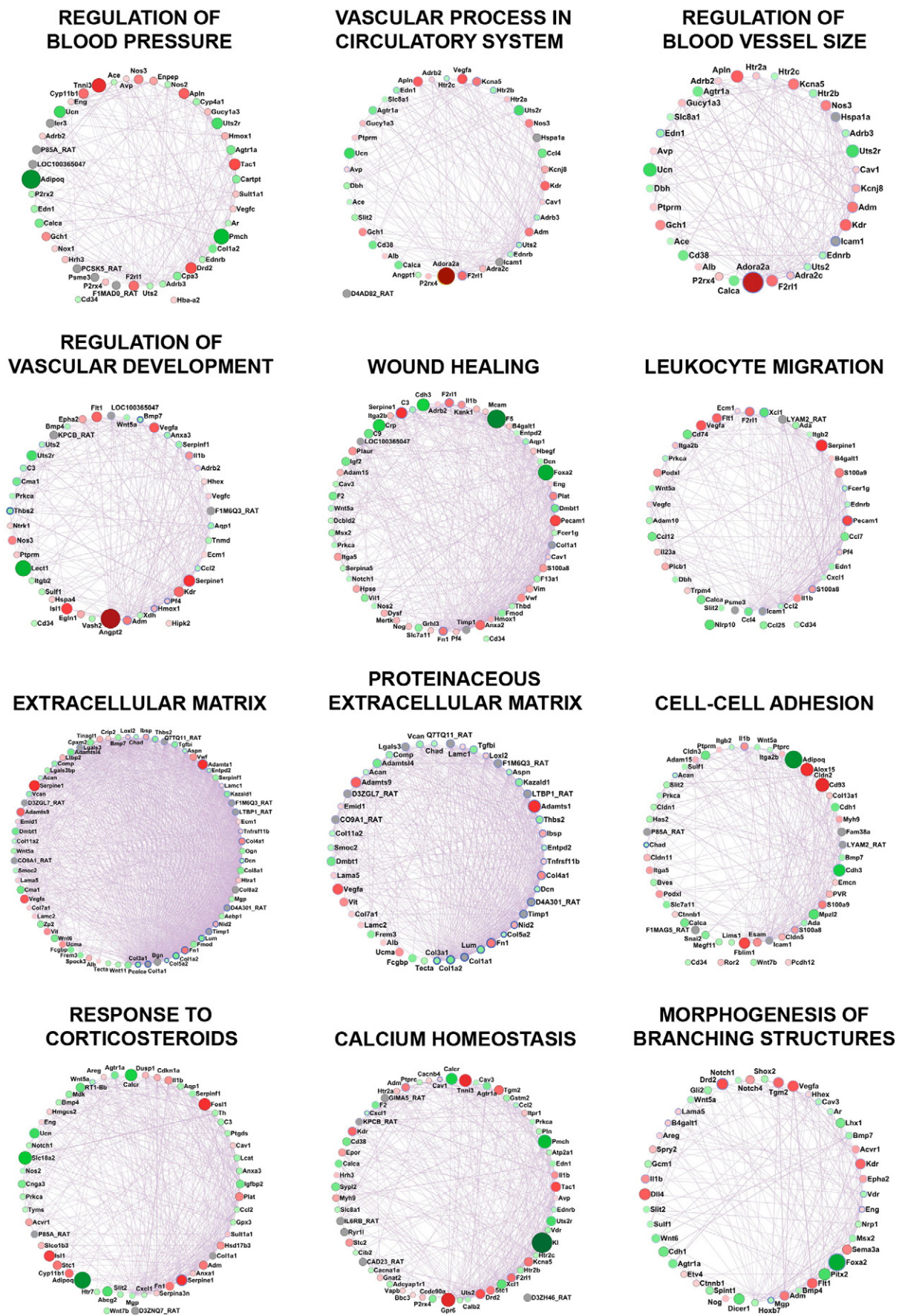
Fig. 3. Enrichment of non-redundant biological processes related to vascular injury during early phases (Day 1) of HH. The list of differentially expressed genes (Hippocampus, day 1 post HH) was subjected to analysis employing 'GeneMANIA' and the networks representing significantly enriched biological processes were represented as 'Degree sorted circular view'.

Table 1
Panther and KEGG pathways (Day 1).

Panther Pathways

Term	Count	P Value	Genes	Fold change (Log2)
P00011:Blood coagulation	16	5.77E–04	SERPINE1	2.8443542
			TFPI	1.7853713
			F2RL2	1.7642052
			PROCR	1.7160616
			PLAT	1.6604576
			VWF	1.4912715
			PLAUR	1.453474
			ITGA2B	0.8921404
			THBD	−0.7324126
			F13A1	−0.9336469
			SERPINF1	−1.0370221
			GP1BA	−1.2040944
			MUG2	−1.3793478
			F2	−1.446238
			SERPIND1	−3.5333004
			F5	−4.70774
P05912:Dopamine receptor mediated signaling pathway	19	0.002892104	PPP1R1B	2.3757234
			DRD2	2.36874
			GRAP	1.8972919
			CLIC1	1.2507586
			FLNB	0.9297929
			EPB4.1	0.8747859
			GNG11	0.8746779
			EPB4.1L5	0.6921451
			COMTD1	−0.7163787
			HDC	−0.7939477
			TH	−0.8683033
			DBH	−0.8810172
			LOC689709	−0.9149811
			DRD4	−1.4644895
			DDC	−2.2620616
			TPH1	−2.763118
			CLIC6	−3.125873
			SLC18A2	−3.1415696
			SLC6A3	−7.033893
P00019:Endothelin signaling pathway	21	0.003854266	NOS3	1.6831317
			ADCY5	1.2960057
			PIK3CD	1.271533
			ADCY4	1.1854753
			PLCB1	1.1200645
			RET	1.100955
			ADCY10	0.9667928
			PLA2G4E	0.93243885
			PKN3	0.88681936
			PRKCB	0.8609204
			ITPR1	0.8332429
			AKT2	0.7436042
			RPS6KA5	0.7115321
			PIK3R1	0.6818552
			ECEL1	0.6579509
			PRKCA	−0.7844
			PRKCG	−0.7435055
			NOS2	−0.7568853
			EDNRB	−0.7804198
			EDN1	−0.9989674
			GNA14	−1.1019769
P00026:Heterotrimeric G–protein signaling pathway–Gi alpha and Gs alpha mediated pathway	28	0.021559023	ADORA2A	4.596356
			RGS9	3.3028097
			HTR1D	2.4813447
			DRD2	2.36874
			RGS18	2.0005836
			GNG7	1.457036
			ADCY5	1.2960057
			ADCY4	1.1854753
			RET	1.100955
			PYGL	0.98676443
			GYS2	0.951998
			ADRA2C	0.9169922
			GNG11	0.8746779
			HRH3	0.84554243
			HTR2A	0.8191047
			RGS11	0.7829354
			GNAL	0.7655735
			CREM	0.74777603
			ADRB2	0.67456627
			HTR5B	−0.68358994
			KCNJ9	−0.70458364
			HTR2C	−0.71320677
			HTR7	−0.8106084
			ADRB3	−0.85165596
			HTR2B	−0.97994566
			GNRHR	−1.1969903
			LOC685513	−1.2585919
			DRD4	−1.4644895
P00014:Cholesterol biosynthesis	6	0.034031065	HMGCS2	0.6745615
			RGD1561594	−0.6385875
			RGD1560208	−0.66789436
			HMGCS1	−0.712842
			FDPS	−0.7152734
			IDI1	−0.8051386
			MVD	−1.1668863
P05911:Angiotensin I–stimulated I signaling through G proteins and beta–arrestin	11	0.05914163	GNG7	1.457036
			PLCB1	1.1200645
			GNG11	0.8746779
			PRKCB	0.8609204
			ITPR1	0.8332429
			PRKCG	−0.7435055
			PRKCA	−0.7844
			RHOD	−1.0399897
			RSA–14–44	−1.2486258
			LOC685513	−1.2585919
			AGTR1A	−1.5141063
P00034:Integrin signalling pathway	33	0.060880193	GRAP	1.8972919
			FN1	1.8335872
			ABL1	1.6461685
			COL4A1	1.5585132
			COL17A1	1.5140443
			COL4A2	1.4545646
			ITGA5	1.3283875
			PIK3CD	1.271533

Pathway	n	p-value	Gene	Value
P04371:5–Hydroxytryptamine biosynthesis	4	0.021548497	HDC	–0.7939477
			TH	–0.8683033
			DDC	–2.2620616
			TPH1	–2.763118
			ACTN1	0.7967496
			COL13A1	0.7933414
			LAMC2	0.7582145
			COL7A1	0.7147064
			CAV1	0.7034116
			LOC685488	0.70186234
			LAMA5	0.69947433
			PIK3R1	0.6818552
			LOC679711	0.67974806
			LAMC1	0.60901594
			ITGB2	–0.6738734
			COL11A2	–0.69414854
			COL9A1	–0.6942651
			COL5A2	–0.7076521
			LIMS1	–0.75985765
			COL14A1	–0.7926967
			LOC363337	–0.9194498
			COL10A1	–1.0163882
			RHOD	–1.0399897
			COL3A1	–1.1294589
			RSA–14–44	–1.2486258
			COL8A1	–1.3336091
			COL1A2	–1.4690781
			ITGB6	–1.8243966
P00001:Adrenaline and noradrenaline biosynthesis	8	0.078337129	COMTD1	–0.7163787
			HDC	–0.7939477
			TH	–0.8683033
			DBH	–0.8810172
			DDC	–2.2620616
			TPH1	–2.763118
			SLC18A2	–3.1415696
			SLC6A3	–7.033893
P00027:Heterotrimeric G–protein signaling pathway–Gq alpha and Go alpha mediated pathway	22	0.096524454	ADORA2A	4.596356
			RGS9	3.3028097
			RASGRP2	3.1607108
			DRD2	2.36874
			RGS18	2.0005836
			GNG7	1.457036
			PLCB1	1.1200645
			GNG11	0.8746779
			PRKCB	0.8609204
			ITPR1	0.8332429
			RGS11	0.7829354
			RAP1GAP	0.7810283
			ARHGEF11	0.7358856
			CACNA1A	–0.61188555
			KCNJ9	–0.70458364
			PRKCG	–0.7435055
			PRKCA	–0.7844
			RHOD	–1.0399897
			GNRHR	–1.1969903
			RSA–14–44	–1.2486258
			LOC685513	–1.2585919
			DRD4	–1.4644895
			ARPC1B	1.1639299
			FLNB	0.9297929
			ITGA2B	0.8921404
			LOC683963	0.8268299
			LOC367516	0.8187952
			ITGA2B	0.8921404
			LAMC2	0.7582145
			LAMA5	0.69947433
			LAMC1	0.60901594
			LOC681309	–0.6848483
			COL11A2	–0.69414854
			COL5A2	–0.7076521
			CHAD	–0.73622775
			COMP	–1.0570307
			COL3A1	–1.1294589
			THBS2	–1.2029161
			GP1BA	–1.2040944
			COL1A2	–1.4690781
			ITGB6	–1.8243966
			SPP1	–2.052303
rno04510:Focal adhesion	39	1.13E–04	VEGFA	2.246623
			FLT1	2.0796452
			KDR	2.040841
			SHC4	1.966058
			FN1	1.8335872
			COL4A1	1.5585132
			VWF	1.4912715
			COL4A2	1.4545646
			ITGA5	1.3283875
			PIK3CD	1.271533
			IBSP	1.1771476
			FLNB	0.9297929
			ITGA2B	0.8921404
			PRKCB	0.8609204
			LOC501280	0.8587365
			ACTN1	0.7967496
			BIRC3	0.77315354
			LAMC2	0.7582145
			AKT2	0.7436042
			VEGFC	0.7373686
			CAV1	0.7034116
			LAMA5	0.69947433
			CTNNB1	0.6886425
			PIK3R1	0.6818552
			LAMC1	0.60901594
			LOC681309	–0.6848483
			COL11A2	–0.69414854
			COL5A2	–0.7076521
			CHAD	–0.73622775
			PRKCG	–0.7435055
			CAV3	–0.74353504
			PRKCA	–0.7844
			COMP	–1.0570307
			COL3A1	–1.1294589
			THBS2	–1.2029161
			RSA–14–44	–1.2486258
			COL1A2	–1.4690781
			ITGB6	–1.8243966
			SPP1	–2.052303
rno04540:Gap junction	20	5.86E–04	DRD2	2.36874
			TUBB6	1.5840988
			ADCY5	1.2960057
			ADCY4	1.1854753
			GUCY1B3	1.1435361

KEGG Pathways

Pathway	Count	p-value	Gene	Value
rno04512:ECM–receptor interaction	22	6.63E–05	FN1	1.8335872
			COL4A1	1.5585132
			VWF	1.4912715
			COL4A2	1.4545646
			ITGA5	1.3283875
			IBSP	1.1771476
			CD36	1.1001186
			TUBB3	–0.76714754
			PRKCA	–0.7844
			TUBA1C	–0.8032026
			TUBA8	–0.96178055
			HTR2B	–0.97994566
rno00100:Steroid biosynthesis	8	0.001061499	HSD17B7	–0.6217203
			NSDHL	–0.7051382
			SQLE	–0.7577033
			CYP51	–0.83079195
			DHCR24	–0.84135437
			TM7SF2	–0.95091915
			DHCR7	–0.96000814
			SOAT2	–2.136528
rno04514:Cell adhesion molecules (CAMs)	28	0.002969832	PECAM1	2.4711046
			ESAM	1.5237026
			RT1–N3	1.5197141
			SELE	1.2301354
			PVR	1.0194507
			CLDN5	1.0137239
			RT1–N1	1.0022795
			CLDN11	0.9885502
			MPZL1	0.9415822
			F11R	0.81968594
			NFASC	0.7557125
			PTPRM	0.7454734
			PTPRC	–0.66197205
			ITGB2	–0.6738734
			CD34	–0.6803694
			NRXN2	–0.7213731
			CLDN1	–0.7981963
			MPZ	–0.9497359
			RT1–T18	–0.9589927
			RT1–DB1	–1.0709939
			VCAN	–1.0723538
			RT1–DA	–1.2743809
			CDH1	–1.6283634
			CLDN3	–1.6335094
			RT1–BB	–1.8330176
			CDH3	–2.8483317
			GLYCAM1	–5.4058876
			CLDN2	–5.5740385
rno04614:Renin–angiotensin system	8	0.003190858	MME	1.4994779
			ENPEP	1.268023
			MAS1	–0.63812685
			ACE	–0.67749214
			CPA3	–1.2984309
			MCPT10	–1.3249769
			AGTR1A	–1.5141063
			CMA1	–1.5416882
			PLCB1	1.1200645
			GUCY1A3	0.8903427
			PRKCB	0.8609204
			ITPR1	0.8332429
			HTR2A	0.8191047
			TUBA4A	–0.6209159
			TUBA1B	–0.657351
			HTR2C	–0.71320677
			PRKCG	–0.7435055
			TUBB5	–0.75383997
			PRKCA	–0.7844
			CLDN1	–0.7981963
			RSA–14–44	–1.2486258
			TXK	–1.5115731
			CLDN3	–1.6335094
			CLDN2	–5.5740385
rno04020:Calcium signaling pathway	32	0.004521905	ADORA2A	4.596356
			NOS3	1.6831317
			ADCY4	1.1854753
			PLCB1	1.1200645
			PDE1B	1.0738964
			PRKCB	0.8609204
			P2RX4	0.84352183
			ITPR1	0.8332429
			HTR2A	0.8191047
			GNAL	0.7655735
			ADRB2	0.67456627
			CAMK4	0.6577492
			CACNA1A	–0.61188555
			HTR5B	–0.68358994
			ATP2A1	–0.6867933
			HTR2C	–0.71320677
			SLC8A1	–0.7239742
			P2RX2	–0.73717046
			PRKCG	–0.7435055
			NOS2	–0.7568853
			PLN	–0.7792568
			EDNRB	–0.7804198
			PRKCA	–0.7844
			HTR7	–0.8106084
			ADRB3	–0.85165596
			RYR1	–0.924412
			HTR2B	–0.97994566
			GNA14	–1.1019769
			ATP2A3	–1.125823
			NTSR1	–1.1850097
			AGTR1A	–1.5141063
			CD38	–1.5396469
rno05222:Small cell lung cancer	17	0.011903225	FN1	1.8335872
			COL4A1	1.5585132
			COL4A2	1.4545646
			PIK3CD	1.271533
			MAX	0.91229844
			ITGA2B	0.8921404
			RARB	0.8681197
			BIRC3	0.77315354
			LOC687813	0.7597294
			LAMC2	0.7582145
			AKT2	0.7436042
			LAMA5	0.69947433
			PIK3R1	0.6818552

Pathway	Count	p-value	Gene	Value
rno04670:Leukocyte transendothelial migration	23	0.003879689	PECAM1	2.4711046
			ITK	2.339603
			ESAM	1.5237026
			PIK3CD	1.271533
			CLDN5	1.0137239
			RAPGEF4	0.9965453
			CLDN11	0.9885502
			PRKCB	0.8609204
			LOC501280	0.8587365
			F11R	0.81968594
			ACTN1	0.7967496
			CTNNA1	0.7173381
			CTNNB1	0.6886425
			PIK3R1	0.6818552
			NOX1	0.67736244
			ITGB2	−0.6738734
			PRKCG	−0.7435055
			KCNMB2	−0.76567173
			PRKCA	−0.7844
			ACTG2	−0.865891
			CYP4A1	−0.95697904
			PLA2G5	−0.96909213
			RSA–14–44	−1.2486258
			AGTR1A	−1.5141063
			CALCRL	−1.6512504
rno04610:Complement and coagulation cascades	14	0.029442743	SERPINE1	2.8443542
			TFPI	1.7853713
			PLAT	1.6604576
			VWF	1.4912715
			PLAUR	1.453474
			C8G	−0.6398494
			SERPINA5	−0.6831827
			THBD	−0.7324126
			F13A1	−0.9336469
			C3	−0.9861479
			F2	−1.446238
			C9	−1.7074528
			SERPIND1	−3.5333004
			F5	−4.70774
rno04062:Chemokine signaling pathway	27	0.034519164	RASGRP2	3.1607108
			ITK	2.339603
			SHC4	1.966058
			GNG7	1.457036
			ADCY5	1.2960057
			PIK3CD	1.271533
			ADCY4	1.1854753
			PLCB1	1.1200645
			CCL6	1.1072657
			IQUB	0.8870621
			GNG11	0.8746779
			PRKCB	0.8609204
			PF4	0.79803133
			AKT2	0.7436042
			PIK3R1	0.6818552
			CXCL1	−0.6154723
			CCL2	−0.74478173
			CXCL9	−0.7801604
			CCL25	−1.196212
			RSA–14–44	−1.2486258
			LOC685513	−1.2585919
			RXRG	0.6225977
			LAMC1	0.60901594
			NOS2	−0.7568853
			PDE11A	−0.839766
rno04270:Vascular smooth muscle contraction	20	0.026360446	ADORA2A	4.596356
			ADCY5	1.2960057
			ADCY4	1.1854753
			GUCY1B3	1.1435361
			PLCB1	1.1200645
			PLA2G4E	0.93243885
			GUCY1A3	0.8903427
			PRKCB	0.8609204
			ITPR1	0.8332429
			ARHGEF11	0.7358856
			RAMP1	0.6719227
			PRKCG	−0.7435055
			HTR7	−0.8106084
			GABRB3	−0.81573105
			ADRB3	−0.85165596
			HCRTR1	−0.86431456
			LPAR2	−0.87759614
			ADCYAP1R1	−0.8814521
			GALR1	−0.9610293
			HTR2B	−0.97994566
			TAAR7B	−1.090653
			NTSR1	−1.1850097
			GNRHR	−1.1969903
			MCPT10	−1.3249769
			F2	−1.446238
			DRD4	−1.4644895
			AGTR1A	−1.5141063
			PTGDRL	−1.6005907
			CALCRL	−1.6512504
			UTS2R	−2.1746721
			CALCR	−2.7912755
			PRLR	−2.7981958
rno00900:Terpenoid backbone biosynthesis	5	0.05205725	HMGCS2	0.6745615
			RGD1561594	−0.6385875
			HMGCS1	−0.712842
			FDPS	−0.7152734
			IDI1	−0.8051386
			MVD	−1.1668863
rno04350:TGF–beta signaling pathway	15	0.065006583	ACVR1	1.245075
			LTBP1	1.0403204
			NOG	0.8657832
			ACVR1C	0.6979971
			ZFYVE9	0.6862364
			FST	0.65952444
			SMAD9	−0.6656542
			LOC681309	−0.6848483
			BMP4	−0.7922139
			DCN	−0.81510496
			BMP7	−0.9723568
			COMP	−1.0570307
			THBS2	−1.2029161
			RSA–14–44	−1.2486258
			PITX2	−2.1505985

			CCL7	−1.4378674
			CXCL11	−1.544837
			CCL12	−1.5502553
			CCL4	−1.5722265
			CCL1	−1.5840888
			XCL1	−1.8675163
rno04080:Neuroactive ligand–receptor interaction	38	0.038080904	ADORA2A	4.596356
			HTR1D	2.4813447
			DRD2	2.36874
			F2RL1	1.9597049
			F2RL2	1.7642052
			ADRA2C	0.9169922
			GABBR1	0.87944365
			NMUR1	0.85039854
			HRH3	0.84554243
			P2RX4	0.84352183
			HTR2A	0.8191047
			GLRB	0.76673746
			ADRB2	0.67456627
			MAS1	−0.63812685
			HTR5B	−0.68358994
			HTR2C	−0.71320677
			P2RX2	−0.73717046
			EDNRB	−0.7804198

We also performed CD31 staining besides vWF (Fig. 4K & L). Interestingly, these experiments revealed relative increase in CD31-positive regions in response to hypoxia—an observation consistent with reported angiogenic propensity induced by hypoxia. Notably, this data is in keeping with our transcriptome results, which also suggested modulation of angiogenesis-specific networks at all time points studied.

Endothelial dysfunction, erosion of basement membrane and activation of Astrocytes cumulatively suggested perturbation of Glio-Vascular organization—a basic structural unit in brain critically regulating 'BBB function'. To investigate this further, we generated evidence utilizing three independent experimental strategies—aimed at studying structural integrity and functional aspects of BBB. We first performed co-immunofluorescence confocal microscopy with Laminin and Aquaporin 4 (Aqp 4). While Laminin stains basement membrane (BM), Aquaporin 4 stains the Astrocyte end feet. Under normal physiological conditions, Aqp 4 positive Astrocyte end feet stay tightly and intimately clasped to basal lamina via interaction with Agrin. However, any neuro-pathophysiological condition of brain culminating in BBB dysfunction is marked by disruption of this interaction and hence, perturbation of this critical 'Glio-Vascular' structure. This phenomenon is evident as segregation of Laminin and Aqp 4 signals in confocal images. As shown in Fig. 4M and Pearson's correlation between spatial localization of signals from the two fluorophores [representing Aqp 4 and Laminin] in Fig. 4N, we reproducibly observed a distinct segregation of Laminin and Aqp 4 signals in response to 3 days of Hypobaric Hypoxia exposure. This interaction was evidently restored by day 7 of HH exposure suggesting that the propensity for functional loss of BBB was transient, which peaked by day 3 and possibly restored by day 7 of HH response.

The loss of 'BBB function' implies that higher molecular weight proteins including Albumin and Immunoglobulins would cross BBB and accumulate in brain parenchyma. To investigate the same, we performed two different experiments namely, Fluorescein extravasation assay (Fig. 4O) and co-immunofluorescence microscopy to monitor extravascular IgG (in parenchyma) as a function of time (post HH), utilizing anti-CD31 and -IgG antibodies (Fig. 4P). We observed a significant increase in the fluorescein signal from hypoxic rat brain extracts (Fig. 4O) besides clear increase in extravascular IgG (parenchyma) in rat brain sections at day 3 (Fig. 4P). Interestingly, similar to Laminin–Aquaporin 4 co-localization, we observed a relative reversal of these phenomena

by day 7 of HH exposure. Taken together, thus, our data strongly suggested perturbation of BBB function (day 3) following an early brain vascular dysfunction in response to HH.

3.5. Hypobaric Hypoxia Decreases H_2S Levels in Brain and Impedes 'Cue-Dependent' Changes in Cerebral Blood Flow

The decrease in Oxygen concentration in circulation leads to vaso-constriction in pulmonary and systemic circulation but vasodilation in cerebral vasculature through mechanisms grossly termed as 'hypoxic cerebral autoregulation'. Besides functional dependence on intact Glio-Vascular integrity, an elevated production of H_2S during hypoxic conditions regulates vasodilation in brain (autoregulation) via inverse relationship between the activity of enzymes, Cystathionine beta synthase (CBS, involved in H_2S production) and Heme Oxygenase-2 (HO-2, involved in CO production) (Morikawa et al., 2012). Thus, in view of early vaso-modulatory signaling, Glio-vascular perturbation in response to HH (as described in the previous sections) and the central role of H_2S in regulating hypoxic-autoregulation in brain; we sought to measure H_2S levels in rat brain, after 1 day of HH exposure. Interestingly, as shown in Fig. 5A, we reproducibly observed significant decrease in the levels of H_2S in response to 1 day of exposure to HH, raising the possibility of perturbed cerebral autoregulation and H_2S production during HH-induced responses in brain. H_2S exerts its vasodilatory effects through multiple pathways including inhibition of Phosphodiesterase (PDE) activity and increasing Nitric Oxide synthase activity (NOS), which cumulatively increases the levels of cGMP in smooth muscle cells. We, therefore, additionally measured the levels of Nitric Oxide (NO) and cGMP in hypoxic brain tissue after 1 day of exposure to HH. As shown in Fig. 5B & C, we clearly observed significantly lower levels of NO and cGMP in the brain tissues of animals exposed to HH. Taken together, we inferred that HH lowers H_2S levels and as a likely consequence, modulated the level of cGMP. We also exogenously administered a known H_2S donor, NaHS, to the animals, prior to HH exposure. As also shown in Fig. 5A, pretreatment with NaHS maintained the levels of H_2S in rat brain during HH. We additionally tested if the levels of NO and cGMP were also maintained during this condition. Notably, as clearly shown in Fig. 5B & C, NaHS pretreatment culminated in significant increase in the levels of NO and cGMP in the brain during HH (1 day). These results cumulatively raised the possibility that HH-induced down-regulation of H_2S production could modulate 'hypoxic cerebral autoregulation' – likely through involvement of cGMP.

To study the phenomenon (described above) at functional level, we next sought to investigate the relative changes in CBF after 24 h of exposure to hypobaric hypoxia, in animals with or without NaHS pretreatment, employing Laser Doppler Flowmetry (LDF). As shown in Fig. 5D & E, we observed a moderate, but statistically significant, increase in BPU value from animals exposed to 24 h (1 day) of HH (Mean BPU values: 332 in Normoxia & 478 in HH). In striking contrast, animals receiving NaHS (kept in Normoxia or Hypoxia) showed a marked increase in blood perfusion across similar region, as compared to Normoxic or Hypoxic animals without NaHS administration (Mean BPU values: 857 & 1042, respectively), (Fig. 5D & E). Consistent with the possibility raised by observations described in Fig. 5A–C, this data set yielded functional evidence for the role of H_2S in regulating vasodilation and effective increase in CBF—an adaptive advantage under hypoxic conditions.

In view of 'cellular flux-dependence' of the LDF data (BPU), it was likely to be affected by changes in the effective concentration (and thus relative number) of bloods cells traversing a region of measurement. Therefore, systemic increase in concentration of RBCs due to Hematopoiesis/Erythropoiesis or Hemoconcentration was also likely to produce changes in BPU values. Notably, both these phenomena are of relevance under hypoxic settings, though with markedly different time kinetics post HH. While Erythropoiesis sets in significantly late—only to be detected after several days of exposure to HH, Hemoconcentration can be observed as early as 6 h post HH (likely
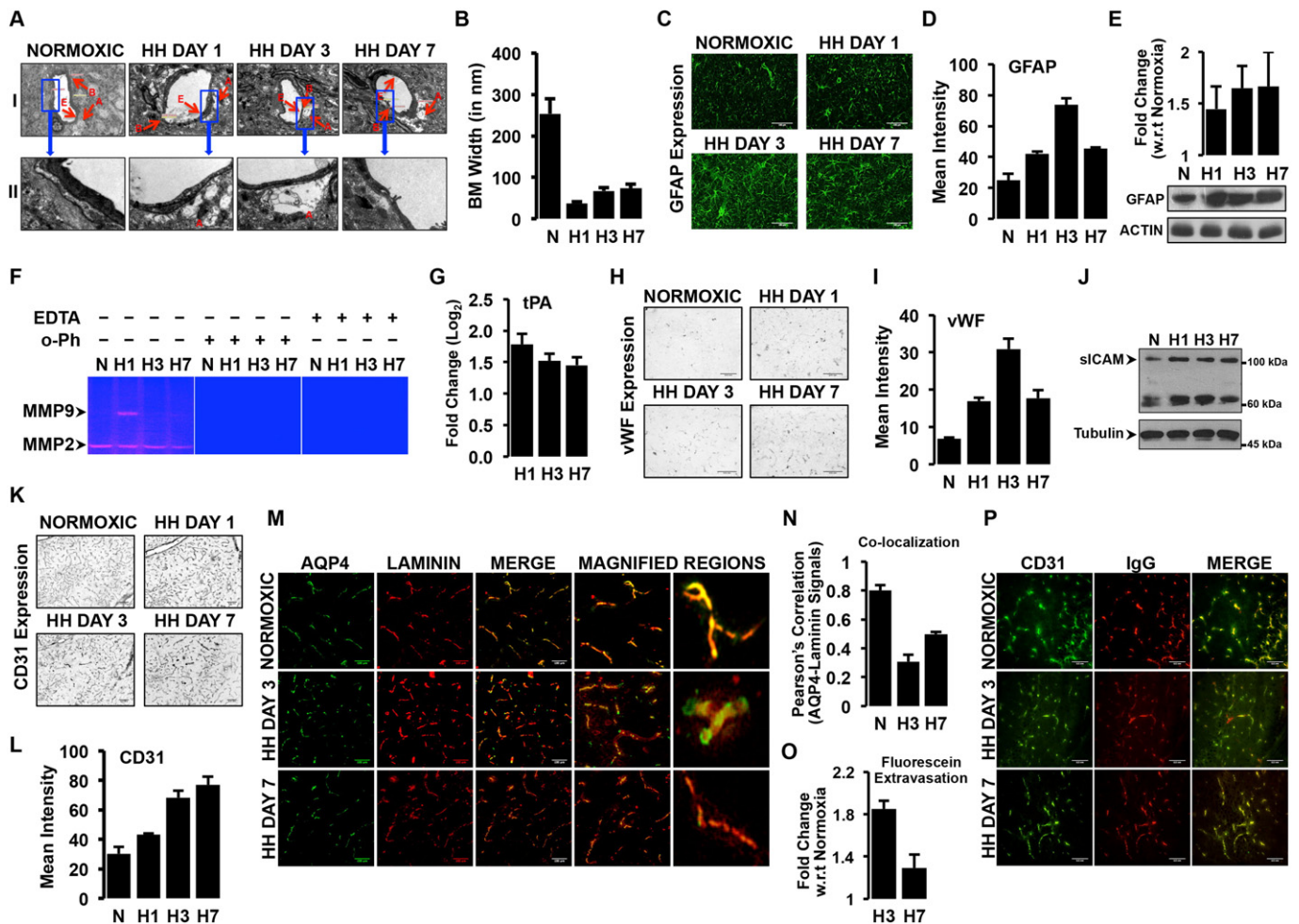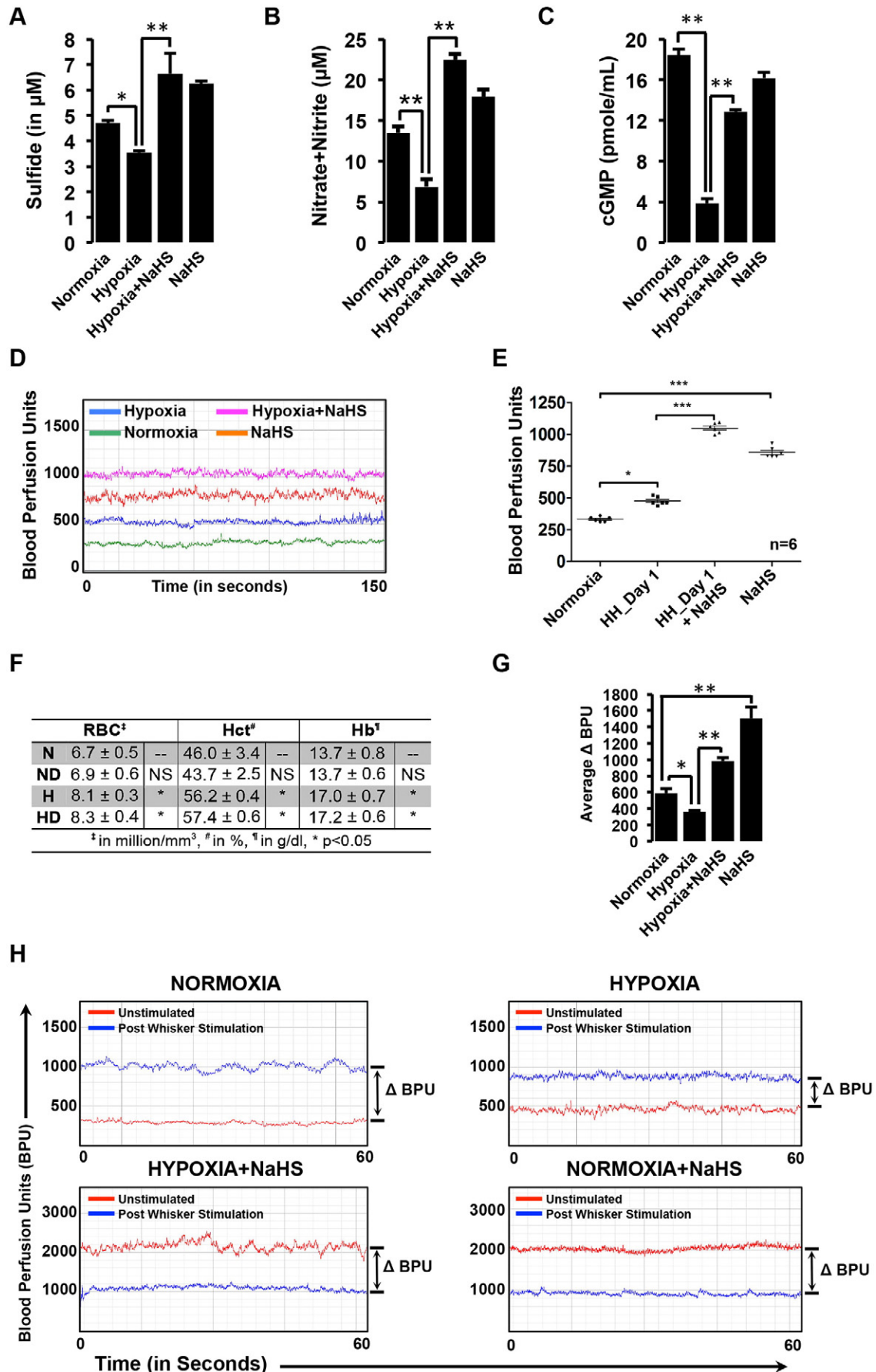
Fig. 4. Ultra-structural and histological evidence for the early 'Glio-Vascular' Unit perturbation A) Transmission electron micrographs of hippocampal sections, post HH exposure (1, 3 & 7 days) (Abbreviations: A: Astrocytes, B: Basement membrane, E: Endothelial cells). Scale bar is 2 μm (I) and 1 μm (II) B) Bar graph showing Basement membrane width (in nm) measured in the electron micrographs of hippocampal regions after HH exposure (Mean ± S.D. was plotted to obtain the graph). C) Immunofluorescence micrographs for GFAP staining, obtained for hippocampal sections using confocal microscopy. Scale bar is shown in each image D) Mean Intensity (indicating GFAP expression), as estimated by Intensity thresholding method and Image J software. E) Western blots showing GFAP expression in the hippocampal region of brain on exposure to HH for 1, 3 & 7 days. The GFAP signal was normalized to β-Actin and average fold change in expression, w.r.t Normoxic is shown as bar graph. F) Representative gelatin zymograms indicating proteolytic activity of MMP-2 (72 kDa) and MMP-9 (92 kDa) at 1, 3 and 7 days post-HH exposure (H1, H3 & H7) in the hippocampus. o-Phenanthroline (zinc-specific chelator) and EDTA (divalent metal ion-chelator) were also included in these experiments to ensure specificity of MMP activity. G) Fold change (Log2) in the expression values (with respect to normoxic control) of tPA transcript at Days 1, 3 & 7, post HH. H) Representative bright field micrographs of Immunohistochemistry staining for vWF in sections from hippocampus, post HH exposure (obtained at 20× magnification). I) Average expression of vWF, as estimated by intensity thresholding method, utilizing Image J software J) Representative western blots for sICAM-1 expression in plasma samples from animals exposed to HH for the indicated period (H1, H3 & H7). The sICAM-1 expression signals were normalized to α-Tubulin, used as internal control and average fold change w.r.t Normoxia shown as bar graph. K) Representative bright field micrographs of Immunohistochemistry staining for CD31 in sections from hippocampus, post HH exposure (20× magnification). L) Average expression of CD31, as estimated by intensity thresholding method, utilizing Image J software M) Co-immunofluorescence confocal micrographs of AQP4 (Green) and Laminin (Red) in the hippocampal sections from Normoxic and HH exposed animals (Days 3 & 7) at 20× magnification. Higher magnification regions from merged images are also shown. Scale bar is included in the images. N) Bar graph representing Pearson's correlation for spatial co- localization of Green (AQP4) and Red (Laminin) channel signals in confocal images O) Fluorescein Extravasation Assay to determine Blood Brain Barrier function. P) Immunofluorescence micrographs from the hippocampal region stained for CD31 (Green) and IgG (Red) under Normoxic as well as HH exposed condition (Days 3 & 7) at 20× magnification. (Abbreviations: N: Normoxic control, H1, H3 & H7: 1, 3 & 7 days, post Hypobaric Hypoxia (HH) exposure) (For interpretation of the references to colour in this figure legend, the reader is referred to the web version of this article.).
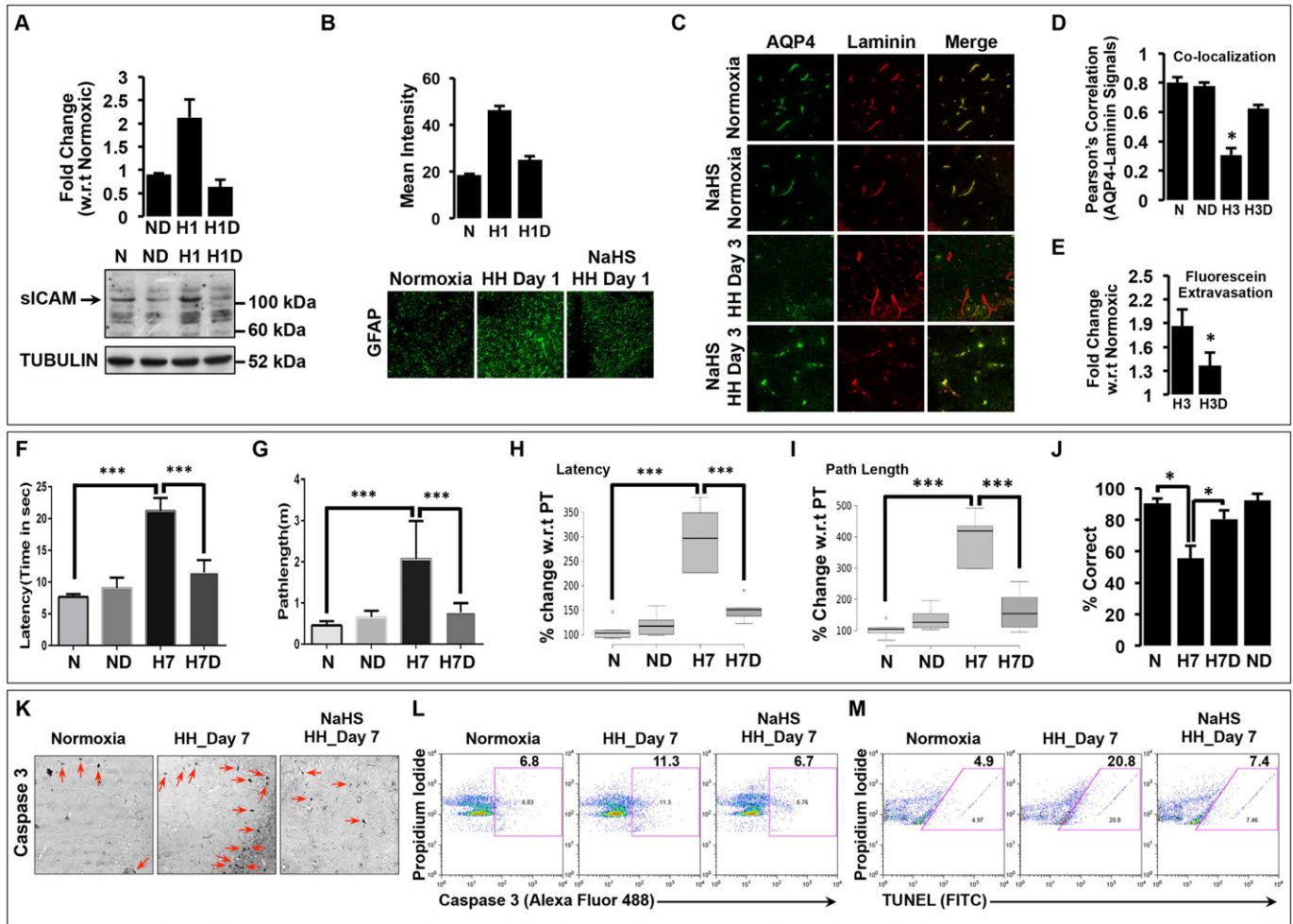
due to prominent diuretic response to increase bicarbonate secretion under hypoxic conditions). It was thus imperative to infer the LDF results (BPU) in conjunction with the relative changes in effective RBC concentrations for all groups. We, therefore, additionally recorded blood cell count in all four groups after 1 day of HH exposure and presented it in Fig. 5F. As expected, we observed nearly 1.2 fold increase in hematocrit values in the animals exposed to hypoxia (irrespective of NaHS treatment) (Fig. 5F). In view of these results, it appears likely that the moderate increase in BPU value of hypoxic animals (not receiving NaHS) is a likely consequence of increased RBC number, as a result of Hemoconcentration. In striking contrast, however, the pronounced increase in BPU value of Normoxic animals receiving NaHS clearly suggests it to be a consequence of vasodilation in brain vasculature (Note that the hematocrit value of this group is comparable to Normoxic

controls in these animals, Fig. 5F). Interestingly, the animals exposed to hypoxia, along with NaHS administration, consistently showed highest BPU values and thus, suggesting possible cumulative effects from hemoconcentration and vasodilation under these conditions.

The results till this stage clearly suggested perturbation of Glio-Vascular homeostasis and function by HH exposure and likely restoration by H₂S augmentation. We, therefore, additionally studied functional hyperemia responses—a measure of Neurovascular coupling—under all four conditions (N, H, ND, HD). For the same, we utilized 'Whisker-Stimulation' protocol (Lecrux et al., 2011) and recorded the changes in CBF (in barrel cortex area) after rhythmic whisker stimulation. We represented the changes in CBF as ΔBPU—the difference in BPU values before and after whisker stimulation. As clearly shown by Fig. 5G & H, we observed a significant reduction in functional hyperemia (average CBF

A

B

C

D

E

F

	RBC‡		Hct#		Hb¶	
N	6.7 ± 0.5	--	46.0 ± 3.4	--	13.7 ± 0.8	--
ND	6.9 ± 0.6	NS	43.7 ± 2.5	NS	13.7 ± 0.6	NS
H	8.1 ± 0.3	*	56.2 ± 0.4	*	17.0 ± 0.7	*
HD	8.3 ± 0.4	*	57.4 ± 0.6	*	17.2 ± 0.6	*
‡in million/mm³, #in %, ¶in g/dl, * p<0.05						

G

H

Fig. 6. Augmentation of endogenous H₂S levels ameliorates Hypobaric Hypoxia induced early gliovascular perturbation A) Representative western blots of sICAM-1 expression in the plasma samples obtained from the indicated groups: Normoxic (N), Normoxic with NaHS pretreatment (ND), Hypoxia (1 day) (H1) & Hypoxia (1 day) pretreated with NaHS (H1D). The protein expression signals were normalized to α-Tubulin (loading control) and average fold change w.r.t Normoxic controls represented as bar graph (Mean ± S.D). B) Immunofluorescence micrographs of GFAP expression in hippocampal sections using confocal microscopy (at 20× objective) for indicated groups: Normoxia & Hypobaric Hypoxia (HH) with/without NaHS pretreatment. Hypobaric Hypoxia (HH) exposure was done for 1 day in these experiments. The micrographs were estimated using Image J and data presented as bar graph in figure C) Co-Immunofluorescence confocal micrographs of AQP4 (green) and Laminin (red) in the hippocampal sections at 20× magnification. The groups are indicated in the figure. Animals in hypoxic groups were exposed to 3 days of HH. D) Bar graph representing Pearson's correlation for spatial co-localization of Green (AQP4) and Red (Laminin) channel signals in confocal images E) Fluorescein Extravasation Assay to determine Blood Brain Barrier function in animals exposed to 3 days of HH, with or without NaHS pretreatment. F) Bar graph representing the Latency parameter (Time taken to reach the platform, in seconds) in MWM test (Mean ± S.D.) for various experimental groups. Animals were kept in Normoxia (N, ND) or exposed to 7 days of HH, with (H7D) or without NaHS (H7) pretreatment. G) Bar graph representing the Path Length parameter (Distance (in m) travelled by the rat to reach the platform) in MWM test (Mean ± S.D.) for said experimental groups (N, ND, H7, H7D). H) Box-and-whisker plot indicating percentage fold change (Mean ± S.D.) in the Latency parameter of the indicated groups during the test w.r.t performance of the same animal in Probe Trial (PT). I) Box-and-whisker plot indicating percentage fold change (Mean ± S.D.) in the Path Length parameter of the indicated groups during the test w.r.t performance of the same animal in Probe Trial (PT). J) Bar graph representing performance of animals in T-Maze test, after 7 days of exposure to HH, with or without NaHS pretreatment. K) Representative regions from bright field micrograph showing cleaved-Caspase 3-positive foci (Immunohistochemistry) from brain sections of animals kept in Normoxia or 7 days of HH, with or without NaHS pretreatment. L) Flow Cytometry analysis of cleaved-Caspase 3 (Alexa fluor 488) positive cells from hippocampal tissues of animals kept in Normoxia or 7 days of HH, with or without NaHS pretreatment. M) Flow Cytometry analysis of TUNEL (FITC) positive cells from hippocampal tissues of animals kept in Normoxia or 7 days of HH, with or without NaHS pretreatment. The significance of differences was evaluated by one-way analysis of variance (***P < 0.001). Bonferroni multiple comparison test was conducted as a post-hoc analysis (For interpretation of the references to colour in this figure legend, the reader is referred to the web version of this article.).

change after whisker stimulation, ΔBPU) under HH conditions as compared to Normoxic controls. Notably, this response was restored when the animals were pretreated with NaHS (H₂S augmented conditions) prior to HH-exposure (Fig. 5G & H). These results, taken together, suggested a likely critical role of H₂S in regulating Neuro-Vascular coupling besides Glio-Vascular homeostasis and function.

Fig. 5. HH-induced perturbation of vasomodulatory gaseous transmitters (H₂S, NO), cGMP and H₂S regulated changes in Cerebral Blood Flow (CBF) in brain. Bar graphs showing A) total sulfide concentration B) NOx (Nitrate & Nitrite) concentration C) cGMP concentration in the brain samples from various groups: Normoxia, Hypoxia, Hypoxia Drug (pretreated with NaHS), Normoxia Drug (pretreated with NaHS). Animals were exposed to Hypobaric Hypoxia for 1 day. The standard curve in each assay was prepared utilizing known concentrations of H₂S, NOx and cGMP. The results are represented as Mean ± S.D. (* P < 0.05, **P < 0.01). D) Overlay of signals obtained from Laser Doppler Flowmetry (indicating cerebral blood flow (CBF)) from Normoxic or Hypoxic animals, with or without H₂S pretreatment. E) Scatter plots of mean blood perfusion units (CBF) values from 6 individual animals within each group (Normoxic, Hypoxic, Hypoxia + NaHS or NaHS alone (Normoxia + NaHS). Median values are also indicated. F) Average values of RBC count, Hematocrit (Hct) and Hemoglobin (Hb) for animals from indicated groups. Respective units are also mentioned below the figure. G) Functional hyperemia responses, studied employing Whisker Stimulation Protocol. The average change in CBF (ΔBPU) was calculated and represented as bar graph (Mean ± S.D). H) Representative overlays of signals obtained from Laser Doppler Flowmetry, before and after whisker stimulation in individual groups (Normoxia, Hypoxia, Hypoxia + NaHS, Normoxia + NaHS). Statistical significance of various parameters shown in the figure was evaluated by one-way analysis of variance (*P < 0.05, **P < 0.01).
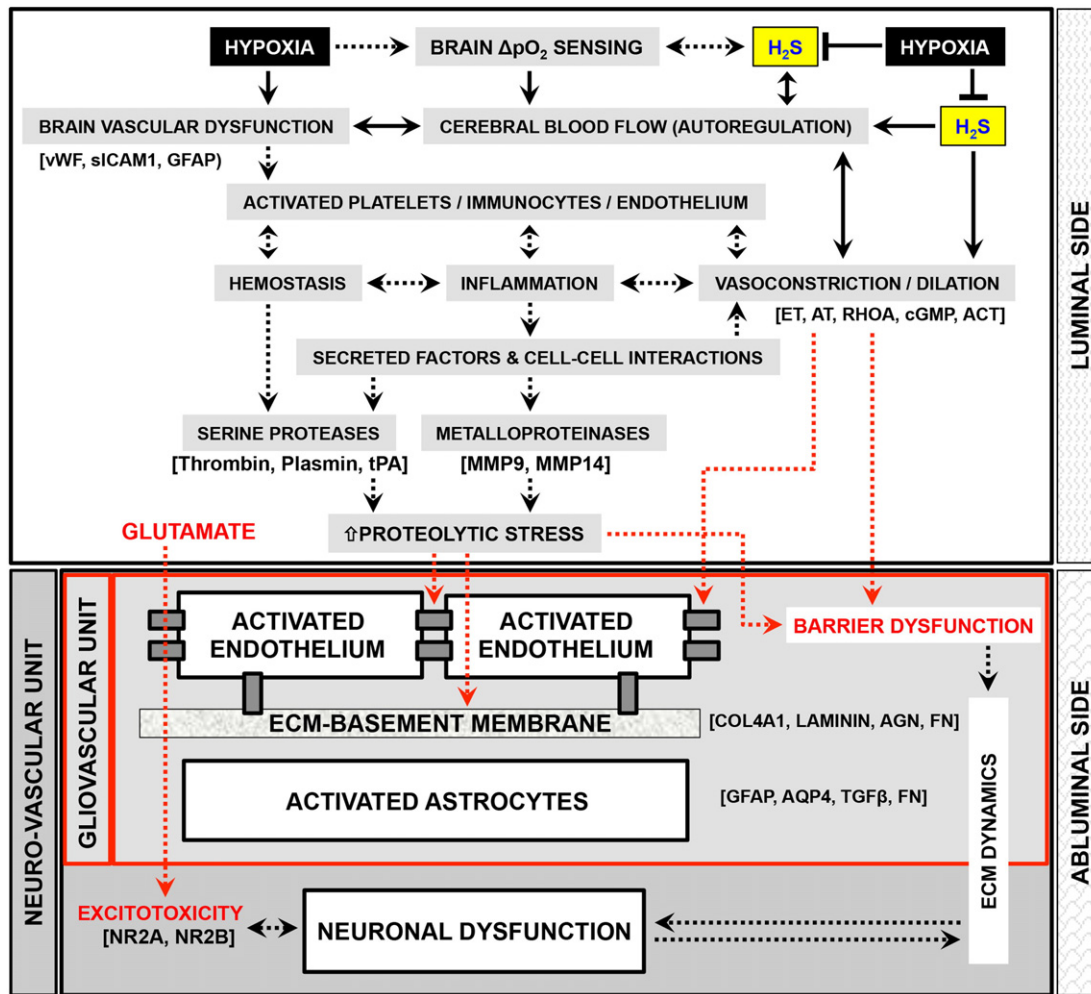
Fig. 7. Proposed integrative working model. The scheme of events deciphered from current study have been schematically represented within a known framework of basic units of function in brain, Neurovascular Units (NVU)—centrally regulating neurophysiological functions and Gliovascular Units—regulating BBB function besides cerebral blood flow (CBF). The brain oxygen sensing mechanism regulates cerebral autoregulation and CBF—likely through steady state levels of H_2S in brain. The absence of sufficient H_2S levels under chronic hypoxic conditions culminates in vascular dysfunction, involving endothelial and blood cell activation (regulating pathways such as hemostasis, inflammatory propensity and vascular tone). These events culminate in increased proteolytic stress (involving proteases such as tPA, MMP9), basement membrane erosion, Astrocyte activation and loss of structural/ functional integrity of Gliovascular units. This likely increases the permeability of molecules such as glutamate (present at much higher concentrations in circulation than in brain) and thus, culminating in neuronal damage concomitant with neuro-pathophysiological effects such as cognitive impairment.

3.6. H2S Augmentation Prevents Hypobaric Hypoxia Induced Neuro-Pathophysiological Effects

We next sought to investigate if HH-induced decrease in the level of H_2S was causally linked to neuro-pathophysiological responses observed during these conditions. For the same, we re-investigated a number of parameters in the animals, pretreated with NaHS to maintain steady state levels of H_2S during HH exposure. For investigating HH-induced Endothelial dysfunction, we performed western blotting for sICAM-1 in plasma samples from animals exposed to HH, with/without NaHS pretreatment. As shown in Fig. 6A, we observed significantly lower levels of sICAM in HH-exposed animals, pretreated with NaHS. This observation clearly suggested efficacy of H_2S in regulating endothelial activation. We next examined the expression of GFAP in brain sections of these animals as a measure of Astrocyte activation. As clearly evident from Fig. 6B, HH-induced increase in the expression of GFAP was markedly abolished in animals receiving NaHS, prior to hypoxia exposure, suggesting amelioration of HH-induced early Astrocyte activation under these conditions.

Since we had observed that the early perturbation of 'Glio-Vascular Units' & BBB function (at day 3) precedes neuronal dysfunction in our model system, we again performed assays to study structural and functional integrity of BBB in H_2S supplemented animals exposed to HH. We first performed confocal microscopy to establish Laminin–Aquaporin 4 co-localization (measure of Glio-Vascular structural integrity) in brain sections of animals pretreated with NaHS, prior to 3 days of HH exposure. As shown in Fig. 6C & D; in striking contrast to the animals exposed to HH without NaHS, the Laminin–Aquaporin 4 signals co-localized significantly higher in the brain sections of animals receiving NaHS, prior to HH. Notably, similar observations were made in Fluorescein extravasation assay (Fig. 6E), where Fluorescein signal was significantly lower in hypoxic group (3 days), receiving NaHS and thus, suggesting preservation of BBB functionality in these animals. We thus inferred that NaHS-mediated maintenance of H_2S levels prevented HH-induced loss of Glio-Vascular function and homeostasis.

To investigate the effects of H_2S maintenance on neuro-physiological functioning; we, next, performed Morris Water Maze and T-Maze tests in the animals exposed to 7 days of hypobaric hypoxia, with/without NaHS pretreatment. As shown in Fig. 6F–I, pre-treatment with NaHS prevented spatial reference memory deficit in response to 7 days of HH exposure. Similar results were obtained in rewarded alternation tasks studied by elevated T-maze assay (Fig. 6J). These results, taken

together, suggested that the maintenance of H_2S levels under Hypobaric Hypoxia conditions alleviates its patho-physiological effects on memory.

We additionally tested if the preservation of neuro-physiological effects was mediated by prevention of neuronal apoptosis (described in Fig. 1 for HH exposure). We studied the same in independent experiments involving multiple technical approaches. The panels in Fig. 6K show IHC staining for cleaved-Caspase 3 while those in Fig. 6L & M depict flow cytometry based analyses of intracellular cleaved-Caspase 3 (active form) expression and TUNEL assay in the cells isolated from hippocampus of animals exposed to 7 days of HH, with or without NaHS pretreatment. These experiments strongly suggested prevention of HH-induced apoptosis of neuronal cells in animals pretreated with NaHS.

The results described in this section, taken together, clearly suggested that H_2S is critical for brain vascular homeostasis during HH and the maintenance of its levels, during these conditions, preserves Glio-Vascular integrity, neuronal viability and thus, alleviation of HH-induced patho-physiological effects in brain.

Fig. 7 schematically depicts the working hypothesis, as inferred from various spatio- temporal events deciphered from the current study, integrated to the established framework of specific units of function in brain, Neuro-Vascular and Glio-Vascular units (see figure legend for details).

4. Discussion

The present study addressed critical issues pertaining to the origin/mechanism of neuro- pathological effects of Hypobaric Hypoxia and interestingly, described a promising interventional strategy for preserving Glio-Vascular homeostasis. Despite several decades of neurophysiological research involving both human subjects and animal models, the precise patho-etiology of chronic effects of high altitude (HA) on memory and cognition continued to remain elusive. The complexity arising due to concomitant, spatio-temporal responses of heterogeneous brain cell types—each having different threshold for adaptation to hypoxia and responses to paracrine factors (due to systemic distress) in circulation—posed a major limitation for mechanistic understanding of this complex phenomenon. Our current study, employing an animal model of Hypobaric Hypoxia and systems level analysis, rendered a unique advantage in this regard. The time-series experiments have proven supremacy over static measurements for inferring and modeling dynamic biological processes (Bar-Joseph et al., 2012). The potential of such datasets is however, harnessed to its fullest with the analysis assuming a holistic view such that the network of putative co-expressed genes is deciphered on time dimension. The unbiased statistical coexpression networks were therefore effective in distinguishing temporal patterns of responses. Our study clearly indicated that the early phase of responses to HH involved Glio-Vascular dysfunction, which likely progressed to perturb neuronal processes during later durations. In general, virtually all forms of pathophysiological conditions affecting brain originate at a specific level in the modular Neuro-Vascular assembly (involving cerebro- vasculature, astrocytes, neurons) and eventually transmitted to other components in these 'units of function'—central to all neurological processes. Thus, identifying the origin of perturbation in our study proved to be of unparalleled significance in revealing a potential interventional approach targeting deleterious effects of HA.

Interestingly, the phenomenon deciphered from our model system appears to be analogous to findings reported for non-lethal forms of High Altitude Cerebral Edema (HACE) in human subjects. The transcriptome signatures of brain at day 1 (post HH) in conjunction with various histological and ultra structural evidences described in our study (Figs. 3 & 4), unambiguously suggested cascade of events involving vascular dysfunction/injury, inflammation and hemostatic responses. Similar phenomenon of micro-hemorrhagic injury (conceivably involving vascular injury followed by hemostatic processes) has also been observed in high-resolution MRI studies involving human subjects diagnosed with non-lethal form of HACE (Kallenberg et al., 2008; Schommer et al., 2013). It thus appears logical to conclude that perturbation of brain vascular homeostasis during acute phases could be the common route to human ailments observed at HA and chronic neuropathological effects of HH in our animal model. Further, in corollary, this inference also underscores the relevance of the molecular circuitry deciphered from our present study for general mechanistic reconstruction of brain responses to HA.

During recent years, certain working hypotheses had been put forth to explain HA-induced loss of BBB integrity during severe clinical conditions such as HACE (High Altitude Cerebral Edema). While one proposition suggested likely perturbation of hemodynamics in brain, originating from imbalance of cerebral inflow exceeding outflow capacity, as a putative trigger of BBB disruption (Willmann et al., 2014; Wilson et al., 2013, 2011, 2009); the other hypothesis emphasized a vital role of soluble factors including VEGF, VEGFR (Schoch et al., 2002; Tissot van Patot et al., 2005; Xu and Severinghaus, 1998) and ROS (Patir et al., 2012) in increasing vascular permeability. Our present data set is particularly interesting for HH (or HA)-induced vascular dysfunction and as discussed below, suggests concomitant modulation of multiple, interacting biological pathways—each capable of affecting vascular permeability. First, our gene expression data strikingly revealed distinct networks/pathways involved in regulation of cerebro-vascular tone. This included genes composing signaling cascade downstream of Adenosine A2A receptor (ADORA2A), Angiotensin II, Endothelin and Catecholamines (Adrenalin and Noradrenalin) (Fig. 3 & Table 1). It thus appears likely that the resultant of such vasomodulatory cues regulates CBF and brain perfusion during HH. Second, we observed decreased levels of two key vasomodulatory gaseous mediators (NO & H_2S) during early phases of response to HH. Intriguing, further, H_2S levels appeared to be causally linked to those of NO, and cGMP—a key second messenger known to regulate Calcium sensitivity/Vascular tone. These important observations, in conjunction with actual CBF measurements under various conditions (Fig. 5), likely indicate insufficient hypoxic cerebral autoregulation—in an H_2S-dependent manner—during hypobaric hypoxia. Third, the global gene expression signatures at day 1, post HH, suggested up-regulation of VEGF transcript along with distinct VEGF-responsive and interacting gene networks. As noted above, besides modulating angiogenic response, VEGF signaling appears to increase vascular leakage in response to hypoxia (Schoch et al., 2002). Fourth, the 'Proteolytic imbalance' under these conditions, as evident from basement membrane erosion and substrate zymography in our study, can plausibly aggravate vascular leakage. This phenomenon merits consideration since a critical role of proteases, including tPA, Urokinase and MMPs, have been implicated for breakdown of ECM proteins and resulting BBB dysfunction during ischemic injury (Hermann and ElAli, 2012; Rosell and Lo, 2008; Yepes et al., 2009). Also, the degradation of Laminin—in a plasmin/tPA-dependent manner—precedes excitotoxicity damage to hippocampal neurons (Chen and Strickland, 1997). Finally, our array dataset was also reminiscent of increased expression of several pro-inflammatory mediators and pathways, known to culminate in endothelial activation and weakening of barrier function. Though, within the limitations of our current dataset, it is difficult to examine the temporal contributions of individual processes during loss of BBB integrity, these phenomena are likely to have cumulative, 'feed forward' influence on vascular permeability. We propose that the resultant effects of such pathways govern the severity and extent of vascular dysfunction during HH. In a recent report, interestingly, we inferred a rather similar scheme of events from global gene expression analysis in human individuals diagnosed with high altitude pulmonary edema (HAPE)—another clinical condition, principally originating from vascular dysfunction (Sharma et al., 2014). Taken together, vascular homeostasis appears to constitute the *Achilles heels* of adaptation to high altitude with unifying underlying mechanisms in multiple organ systems.

Remarkably, despite employing a specific region of brain for the present study, the nature of early perturbation induced by HH does not appear to be region-specific. Arguably, though, its magnitude and manifestations may vary in individual regions owing to differences in anatomical organization. Yet the most common patho-physiological manifestation of HH includes loss of functions related to hippocampus (memory and cognition). We suggest that such regio-specific effects could arise due to intrinsic vulnerability of individual regions of brain to BBB dysfunction. As an example, a likely consequence of loss of BBB function would, arguably, be increase in concentration of Glutamate in brain interstitial tissue. This key excitatory amino acid is present at a concentration of ~100 μM in plasma and <1 μM in brain interstitial fluid (Abbott et al., 2006). The neurons—which are typically located 8–20 μm away from brain capillaries (Abbott et al., 2006)—would thus be exposed to excitotoxicity damage in the event of loss of BBB function. In keeping with this proposition, the predominance of glutamatergic neurons in hippocampus could explain its vulnerability to HH and at least in part, effects of HH on memory (Koundal et al., 2014; Maiti et al., 2008; Pulsinelli, 1985). Summarily, these arguments further support the possibility of 'secondary' damage to neurons during hypobaric hypoxia-induced memory dysfunction and also, accentuate interventional strategies aimed to preserve brain vascular homeostasis under these settings.

It is increasingly being recognized that the triggers of disease in neuro-degeneration may also provide cues for endogenous compensation and recovery (Arai et al., 2009; Lo, 2010). Hence, an effective strategy should not only counteract the primary cause of degeneration but also, complement the processes of endogenous regeneration and preservation under specific triggers (Lo, 2010). Consistent with this hypothesis as well, H_2S augmentation strategy during HH appears distinctively adept because of following reasons: 1) It is fundamentally a more potent regulator of vascular dynamics due to greater diversity of targets and effects (both direct or indirect)—ranging from systemic, cyto-protective, metabolic, biochemical and molecular (Li et al., 2011). Amongst the two gaseous regulators (NO & H_2S) of vascular tone (Coletta et al., 2012; Yang et al., 2008), H_2S seems to have occupied a unique niche. Besides directly regulating vasoconstriction through the activation of KATP channels (Zhao et al., 2001) (abundantly present in cerebral vasculature (Wang et al., 1997)), it regulates NO availability by regulating eNOS activity (King et al., 2014) and also, maintenance of cGMP levels through inhibition of PDE (Bucci et al., 2010). Furthermore, H_2S has been shown to protect against oxidative stress (Kimura and Kimura, 2004) and also, counteract the deleterious effects of electrophilic byproducts of redox signaling (such as 8-nitro-cGMP) directly by electrophile sulfhydration (Nishida et al., 2012). 2) Besides its vasculature-specific effects, H_2S directly exerts its effect on abluminal homeostasis by modulating MMP 9 induced protease stress (Tyagi et al., 2010), Calcium waves in Astrocytes (Nagai et al., 2004) and glial activation (Lee et al., 2010). Possibly, these effects make it a better regulator of BBB function and endows it anti-neuroinflammatory properties. 3) It appears to preserve neurons under pathological conditions arising due to endogenous factors such as β-amyloid (Xuan et al., 2012), homocysteine (Kamat et al., 2013; Li et al., 2014) and glutamate (Qu et al., 2008). 4) Most notably, H_2S appears to promote proliferation and differentiation of neural stem cells under hypoxic challenge (Liu et al., 2014). Taken together, H_2S signaling not only serves as a guardian against NVU insult but also reinforces stimulus-dependent endogenous regeneration pathways, rendering it more potent in curtailing pathological effects of HH.

Notably, the implications of these observations are plausibly of general relevance and likely to find application for other diseases originating from BBB dysfunction as well. Several pathological states of brain including stroke, trauma, infection, pain, multiple sclerosis, HIV, Alzheimer's disease, Parkinson's disease, Epilepsy and brain tumours involve some degree of BBB breakdown and risk of ensuing secondary damage to neurons (Abbott et al., 2006). Not surprisingly, therefore,

strategies for promoting BBB restitution besides possible prevention of its dysfunction during such clinical conditions present an important clinical counteractive strategy. In view of unifying features of HH-induced neuro-pathophysiology and said diseases of brain, we suggest that the mechanisms and interventional approaches, such as H_2S augmentation, deciphered in context to HH would be of possible use for preventing secondary damage to neurons during other pathological states as well.

Supplementary data to this article can be found online at http://dx.doi.org/10.1016/j.ebiom.2016.03.002.

Conflict of interest

The authors have declared that no conflict of interest exists.

Author contributions

MS conceived and coordinated the study. GK, AC, SM, HK, DK, RM, YA, KB, DNP, MS performed and analyzed the experiments. MS, GK, AC wrote the paper. All authors reviewed the results and approved final version of the manuscript.

References

Abbott, N.J., Ronnback, L., Hansson, E., 2006. Astrocyte-endothelial interactions at the blood–brain barrier. Nat. Rev. Neurosci. 7, 41–53.

Ang, A.D., K., A, Giles, G.I., Bhatia, M., 2012. Measuring free tissue sulfide. Adv. Biol. Chem. 2, 360–365.

Arai, K., Jin, G., Navaratna, D., Lo, E.H., 2009. Brain angiogenesis in developmental and pathological processes: neurovascular injury and angiogenic recovery after stroke. FEBS J. 276, 4644–4652.

Bar-Joseph, Z., Gitter, A., Simon, I., 2012. Studying and modelling dynamic biological processes using time-series gene expression data. Nat. Rev. Genet. 13, 552–564.

Bartsch, P., Swenson, E.R., 2013. Clinical practice: acute high-altitude illnesses. N. Engl. J. Med. 368, 2294–2302.

Bouquet, C.A., Gardette, B., Gortan, C., Abraini, J.H., 1999. Psychomotor skills learning under chronic hypoxia. Neuroreport 10, 3093–3099.

Bucci, M., Papapetropoulos, A., Vellecco, V., Zhou, Z., Pyriochou, A., Roussos, C., Roviezzo, F., Brancaleone, V., Cirino, G., 2010. Hydrogen sulfide is an endogenous inhibitor of phosphodiesterase activity. Arterioscler. Thromb. Vasc. Biol. 30, 1998–2004.

Chen, Z.L., Strickland, S., 1997. Neuronal death in the hippocampus is promoted by plasmin-catalyzed degradation of laminin. Cell 91, 917–925.

Coletta, C., Papapetropoulos, A., Erdelyi, K., Olah, G., Modis, K., Panopoulos, P., Asimakopoulou, A., Gero, D., Sharina, I., Martin, E., et al., 2012. Hydrogen sulfide and nitric oxide are mutually dependent in the regulation of angiogenesis and endothelium-dependent vasorelaxation. Proc. Natl. Acad. Sci. U. S. A. 109, 9161–9166.

Deacon, R.M., Rawlins, J.N., 2006. T-maze alternation in the rodent. Nat. Protoc. 1, 7–12.

Dehnert, C., Berger, M.M., Mairbaurl, H., Bartsch, P., 2007. High altitude pulmonary edema: a pressure-induced leak. Respir. Physiol. Neurobiol. 158, 266–273.

Grocott, M., Montgomery, H., Vercueil, A., 2007. High-altitude physiology and pathophysiology: implications and relevance for intensive care medicine. Crit. Care 11, 203.

Hackett, P.H., Roach, R.C., 2001. High-altitude illness. N. Engl. J. Med. 345, 107–114.

Hackett, P.H., Roach, R.C., 2004. High altitude cerebral edema. High Alt. Med. Biol. 5, 136–146.

Hackett, P.H., Yarnell, P.R., Hill, R., Reynard, K., Heit, J., McCormick, J., 1998. High-altitude cerebral edema evaluated with magnetic resonance imaging: clinical correlation and pathophysiology. JAMA 280, 1920–1925.

Harik, S.I., Lust, W.D., Jones, S.C., Lauro, K.L., Pundik, S., LaManna, J.C., 1995. Brain glucose metabolism in hypobaric hypoxia. J. Appl. Physiol. 79, 136–140.

Hermann, D.M., ElAli, A., 2012. The abluminal endothelial membrane in neurovascular remodeling in health and disease. Sci. Signal. 5 (re4).

Hota, S.K., Barhwal, K., Singh, S.B., Sairam, M., Ilavazhagan, G., 2008. NR1 and GluR2 expression mediates excitotoxicity in chronic hypobaric hypoxia. J. Neurosci. Res. 86, 1142–1152.

Imray, C., Wright, A., Subudhi, A., Roach, R., 2010. Acute mountain sickness: pathophysiology, prevention, and treatment. Prog. Cardiovasc. Dis. 52, 467–484.

Kallenberg, K., Dehnert, C., Dorfler, A., Schellinger, P.D., Bailey, D.M., Knauth, M., Bartsch, P.D., 2008. Microhemorrhages in nonfatal high-altitude cerebral edema. J. Cereb. Blood Flow Metab. 28, 1635–1642.

Kamat, P.K., Kalani, A., Givvimani, S., Sathnur, P.B., Tyagi, S.C., Tyagi, N., 2013. Hydrogen sulfide attenuates neurodegeneration and neurovascular dysfunction induced by intracerebral-administered homocysteine in mice. Neuroscience 252, 302–319.

Kimura, Y., Kimura, H., 2004. Hydrogen sulfide protects neurons from oxidative stress. FASEB J. 18, 1165–1167.

King, A.L., Polhemus, D.J., Bhushan, S., Otsuka, H., Kondo, K., Nicholson, C.K., Bradley, J.M., Islam, K.N., Calvert, J.W., Tao, Y.X., et al., 2014. Hydrogen sulfide cytoprotective signaling is endothelial nitric oxide synthase-nitric oxide dependent. Proc. Natl. Acad. Sci. U. S. A. 111, 3182–3187.

Koundal, S., Gandhi, S., Kaur, T., Khushu, S., 2014. Neurometabolic and structural alterations in rat brain due to acute hypobaric hypoxia: in vivo 1H MRS at 7 T. NMR Biomed. 27, 341–347.

Kramer, A.F., Coyne, J.T., Strayer, D.L., 1993. Cognitive function at high altitude. Hum. Factors 35, 329–344.

Ladecola, C., 2013. The pathobiology of vascular dementia. Neuron 80, 844–866.

Langfelder, P., Horvath, S., 2008. WGCNA: an R package for weighted correlation network analysis. BMC Bioinf. 9, 559.

Lecrux, C., Toussay, X., Kocharyan, A., Fernandes, P., Neupane, S., Levesque, M., Plaisier, F., Shmuel, A., Cauli, B., Hamel, E., 2011. Pyramidal neurons are "neurogenic hubs" in the neurovascular coupling response to whisker stimulation. J. Neurosci. 31, 9836–9847.

Lee, M., Tazzari, V., Giustarini, D., Rossi, R., Sparatore, A., Del Soldato, P., McGeer, E., McGeer, P.L., 2010. Effects of hydrogen sulfide-releasing L-DOPA derivatives on glial activation: potential for treating Parkinson disease. J. Biol. Chem. 285, 17318–17328.

Li, L., Rose, P., Moore, P.K., 2011. Hydrogen sulfide and cell signaling. Annu. Rev. Pharmacol. Toxicol. 51, 169–187.

Li, M.H., Tang, J.P., Zhang, P., Li, X., Wang, C.Y., Wei, H.J., Yang, X.F., Zou, W., Tang, X.Q., 2014. Disturbance of endogenous hydrogen sulfide generation and endoplasmic reticulum stress in hippocampus are involved in homocysteine-induced defect in learning and memory of rats. Behav. Brain Res. 262, 35–41.

Liu, D., Wang, Z., Zhan, J., Zhang, Q., Wang, J., Zhang, Q., Xian, X., Luan, Q., Hao, A., 2014. Hydrogen sulfide promotes proliferation and neuronal differentiation of neural stem cells and protects hypoxia-induced decrease in hippocampal neurogenesis. Pharmacol. Biochem. Behav. 116, 55–63.

Lo, E.H., 2010. Degeneration and repair in central nervous system disease. Nat. Med. 16, 1205–1209.

Maiti, P., Singh, S.B., Sharma, A.K., Muthuraju, S., Banerjee, P.K., Ilavazhagan, G., 2006. Hypobaric hypoxia induces oxidative stress in rat brain. Neurochem. Int. 49, 709–716.

Maiti, P., Singh, S.B., Mallick, B., Muthuraju, S., Ilavazhagan, G., 2008. High altitude memory impairment is due to neuronal apoptosis in hippocampus, cortex and striatum. J. Chem. Neuroanat. 36, 227–238.

Mark, L.P., Prost, R.W., Ulmer, J.L., Smith, M.M., Daniels, D.L., Strottmann, J.M., Brown, W.D., Hacein-Bey, L., 2001. Pictorial review of glutamate excitotoxicity: fundamental concepts for neuroimaging. AJNR Am. J. Neuroradiol. 22, 1813–1824.

Morikawa, T., Kajimura, M., Nakamura, T., Hishiki, T., Nakanishi, T., Yukutake, Y., Nagahata, Y., Ishikawa, M., Hattori, K., Takenouchi, T., et al., 2012. Hypoxic regulation of the cerebral microcirculation is mediated by a carbon monoxide-sensitive hydrogen sulfide pathway. Proc. Natl. Acad. Sci. U. S. A. 109, 1293–1298.

Muthuraju, S., Maiti, P., Pati, S., Solanki, P., Sharma, A.K., Singh, S.B., Prasad, D., Ilavazhagan, G., 2011. Role of cholinergic markers on memory function of rats exposed to hypobaric hypoxia. Eur. J. Pharmacol. 672, 96–105.

Nagai, Y., Tsugane, M., Oka, J., Kimura, H., 2004. Hydrogen sulfide induces calcium waves in astrocytes. FASEB J. 18, 557–559.

Nishida, M., Sawa, T., Kitajima, N., Ono, K., Inoue, H., Ihara, H., Motohashi, H., Yamamoto, M., Suematsu, M., Kurose, H., et al., 2012. Hydrogen sulfide anion regulates redox signaling via electrophile sulfhydration. Nat. Chem. Biol. 8, 714–724.

Oldham, M.C., Horvath, S., Geschwind, D.H., 2006. Conservation and evolution of gene coexpression networks in human and chimpanzee brains. Proc. Natl. Acad. Sci. U. S. A. 103, 17973–17978.

Oldham, M.C., Konopka, G., Iwamoto, K., Langfelder, P., Kato, T., Horvath, S., Geschwind, D.H., 2008. Functional organization of the transcriptome in human brain. Nat. Neurosci. 11, 1271–1282.

Patir, H., Sarada, S.K., Singh, S., Mathew, T., Singh, B., Bansal, A., 2012. Quercetin as a prophylactic measure against high altitude cerebral edema. Free Radic. Biol. Med. 53, 659–668.

Phares, T.W., Kean, R.B., Mikheeva, T., Hooper, D.C., 2006. Regional differences in blood–brain barrier permeability changes and inflammation in the apathogenic clearance of virus from the central nervous system. J. Immunol. 176, 7666–7675.

Pulsinelli, W.A., 1985. Selective neuronal vulnerability: morphological and molecular characteristics. Prog. Brain Res. 63, 29–37.

Qu, K., Lee, S.W., Bian, J.S., Low, C.M., Wong, P.T., 2008. Hydrogen sulfide: neurochemistry and neurobiology. Neurochem. Int. 52, 155–165.

Rosell, A., Lo, E.H., 2008. Multiphasic roles for matrix metalloproteinases after stroke. Curr. Opin. Pharmacol. 8, 82–89.

Schoch, H.J., Fischer, S., Marti, H.H., 2002. Hypoxia-induced vascular endothelial growth factor expression causes vascular leakage in the brain. Brain 125, 2549–2557.

Schommer, K., Kallenberg, K., Lutz, K., Bartsch, P., Knauth, M., 2013. Hemosiderin deposition in the brain as footprint of high-altitude cerebral edema. Neurology 81, 1776–1779.

Sharma, M., Singh, S.B., Sarkar, S., 2014. Genome wide expression analysis suggests perturbation of vascular homeostasis during high altitude pulmonary edema. PLoS One 9, e85902.

Sutherland, B.A., Rabie, T., Buchan, A.M., 2014. Laser Doppler flowmetry to measure changes in cerebral blood flow. Methods Mol. Biol. 1135, 237–248.

Sylvester, J.T., Shimoda, L.A., Aaronson, P.I., Ward, J.P., 2012. Hypoxic pulmonary vasoconstriction. Physiol. Rev. 92, 367–520.

Teppema, L.J., Dahan, A., 2010. The ventilatory response to hypoxia in mammals: mechanisms, measurement, and analysis. Physiol. Rev. 90, 675–754.

Tissot van Patot, M.C., Leadbetter, G., Keyes, L.E., Bendrick-Peart, J., Beckey, V.E., Christians, U., Hackett, P., 2005. Greater free plasma VEGF and lower soluble VEGF receptor-1 in acute mountain sickness. J. Appl. Physiol. 98, 1626–1629.

Titus, A.D., Shankaranarayana Rao, B.S., Harsha, H.N., Ramkumar, K., Srikumar, B.N., Singh, S.B., Chattarji, S., Raju, T.R., 2007. Hypobaric hypoxia-induced dendritic atrophy of hippocampal neurons is associated with cognitive impairment in adult rats. Neuroscience 145, 265–278.

Tyagi, N., Givvimani, S., Qipshidze, N., Kundu, S., Kapoor, S., Vacek, J.C., Tyagi, S.C., 2010. Hydrogen sulfide mitigates matrix metalloproteinase-9 activity and neurovascular permeability in hyperhomocysteinemic mice. Neurochem. Int. 56, 301–307.

Virues-Ortega, J., Buela-Casal, G., Garrido, E., Alcazar, B., 2004. Neuropsychological functioning associated with high-altitude exposure. Neuropsychol. Rev. 14, 197–224.

Vorhees, C.V., Williams, M.T., 2006. Morris water maze: procedures for assessing spatial and related forms of learning and memory. Nat. Protoc. 1, 848–858.

Wang, R., Wang, Z., Wu, L., 1997. Carbon monoxide-induced vasorelaxation and the underlying mechanisms. Br. J. Pharmacol. 121, 927–934.

Warde-Farley, D., Donaldson, S.L., Comes, O., Zuberi, K., Badrawi, R., Chao, P., Franz, M., Grouios, C., Kazi, F., Lopes, C.T., et al., 2010. The GeneMANIA prediction server: biological network integration for gene prioritization and predicting gene function. Nucleic Acids Res. 38, W214–W220.

West, J.B., Schoene, Robert B., Milledge, James S., 2007. High Altitude Medicine and Physiology. Hodder Arnold, London.

Willmann, G., Gekeler, F., Schommer, K., Bartsch, P., 2014. Update on high altitude cerebral edema including recent work on the eye. High Alt. Med. Biol. 15, 112–122.

Wilson, M.H., Newman, S., Imray, C.H., 2009. The cerebral effects of ascent to high altitudes. Lancet Neurol. 8, 175–191.

Wilson, M.H., Imray, C.H., Hargens, A.R., 2011. The headache of high altitude and microgravity—similarities with clinical syndromes of cerebral venous hypertension. High Alt. Med. Biol. 12, 379–386.

Wilson, M.H., Davagnanam, I., Holland, G., Dattani, R.S., Tamm, A., Hirani, S.P., Kolfschoten, N., Strycharczuk, L., Green, C., Thornton, J.S., et al., 2013. Cerebral venous system and anatomical predisposition to high-altitude headache. Ann. Neurol. 73, 381–389.

Xu, F., Severinghaus, J.W., 1998. Rat brain VEGF expression in alveolar hypoxia: possible role in high-altitude cerebral edema. J. Appl. Physiol. 85, 53–57.

Xuan, A., Long, D., Li, J., Ji, W., Zhang, M., Hong, L., Liu, J., 2012. Hydrogen sulfide attenuates spatial memory impairment and hippocampal neuroinflammation in beta-amyloid rat model of Alzheimer's disease. J. Neuroinflammation 9, 202.

Yan, X., 2014. Cognitive impairments at high altitudes and adaptation. High Alt. Med. Biol. 15, 141–145.

Yang, G., Wu, L., Jiang, B., Yang, W., Qi, J., Cao, K., Meng, Q., Mustafa, A.K., Mu, W., Zhang, S., et al., 2008. H2S as a physiologic vasorelaxant: hypertension in mice with deletion of cystathionine gamma-lyase. Science 322, 587–590.

Yepes, M., Roussel, B.D., Ali, C., Vivien, D., 2009. Tissue-type plasminogen activator in the ischemic brain: more than a thrombolytic. Trends Neurosci. 32, 48–55.

Zhao, W., Zhang, J., Lu, Y., Wang, R., 2001. The vasorelaxant effect of H(2)S as a novel endogenous gaseous K(ATP) channel opener. EMBO J. 20, 6008–6016.